Hindawi
IET Signal Processing
Volume 2024, Article ID 7768640, 15 pages
https://doi.org/10.1049/2024/7768640

Research Article

Weighted Sum Secrecy Rate Optimization for Cooperative Double-IRS-Assisted Multiuser Network

Shaochuan Yang,[1,2] **Kaizhi Huang**,[1,3] **Hehao Niu**,[4] **Yi Wang**,[2] **Zheng Chu**,[5,6,7] **Gaojie Chen**,[8] **and Zhen Li**[7]

[1]*Wireless Communication Technology Office, Information Engineering University, Zhengzhou 450001, China*
[2]*School of Electronics and Information, Zhengzhou University of Aeronautics, Zhengzhou 450015, China*
[3]*Engineering Research Center of Mobile Network Technologies, Beijing University of Posts and Telecommunications, Beijing 100876, China*
[4]*Sixty-Third Research Institute, National University of Defense Technology, Nanjing 210007, China*
[5]*Institute for Communication Systems (ICS), Home for 5GIC and 6GIC, University of Surrey, Guildford GU2 7XH, SRY, UK*
[6]*Department of Electrical and Electronic Engineering, University of Nottingham Ningbo China, Ningbo 315100, China*
[7]*Shaanxi Key Laboratory of Information Communication Network and Security, Xi'an University of Posts and Telecommunications, Xi'an 710121, Shaanxi, China*
[8]*5GIC and 6GIC, Institute for Communication Systems (ICS), University of Surrey, Guildford GU2 7XH, UK*

Correspondence should be addressed to Kaizhi Huang; huangkaizhi@tsinghua.org.cn and Yi Wang; yiwang@zua.edu.cn

Received 19 November 2023; Revised 21 March 2024; Accepted 28 March 2024; Published 20 April 2024

Academic Editor: Charles Casimiro Cavalcante

Copyright © 2024 Shaochuan Yang et al. This is an open access article distributed under the Creative Commons Attribution License, which permits unrestricted use, distribution, and reproduction in any medium, provided the original work is properly cited.

In this paper, we present a double-intelligent reflecting surfaces (IRS)-assisted multiuser secure system where the inter-IRS channel is considered. In particular, we maximize the weighted sum secrecy rate of the system by jointly optimizing the beamforming vector for transmitted signal and artificial noise at the base station (BS) and the cooperative phase shifts of two IRSs, under the constraints of transmission power at the BS and the unit-modulus phase shift of IRSs. To tackle the nonconvexity of the optimization problem, we first convert the objective function to its concave lower bound by utilizing a novel successive convex approximation technique, then solve the transformed problem iteratively by applying an alternating optimization method. The Lagrange dual method, Karush–Kuhn–Tucker conditions, and alternating direction method of multipliers are applied to develop a low-complexity solution for each subproblem. Finally, simulation results are provided to verify the advantages of the cooperative double-IRS scheme in comparison with the benchmark schemes.

1. Introduction

In order to support emerging wireless services, such as wireless data centers, holographic communication, and immersive XR, 6G network is expected to achieve 100-fold increase in data rate, connection density, and network energy efficiency compared to the 5G network [1]. However, the existing wireless technologies, such as millimeter wave (mmWave), which suffering from significant path loss and attenuation, and massive multiple-input multiple-output (MIMO) requiring active radio-frequency (RF) chains, are unable to further improve the performance of wireless network efficiently (active RF chains result in high energy consumption and hardware cost. Although hybrid beamforming technology can reduce hardware complexity, it still requires active RF chains [2]). Advanced technologies are being developed to satisfy future network requirements. Among them, intelligent reflecting surface (IRS) has recently received much interest from both academic and industry communities for achieving intelligent and programable radio propagation environment cost-effectively [3–5]. Specifically, an IRS is a type of meta-surface that consists of massive low-cost subwavelength reflecting components, each of which can be independently manipulated to adjust the magnitude, phase, frequency, or even polarization of the incident signal [4]. The IRS provides a new degree of freedom by dynamically manipulating the wireless channels to improve

the performance of wireless networks, e.g., channel capacity, throughput, and coverage. Because the IRS does not require any active RF chains, the hardware cost, and energy consumption are significantly lower compared to traditional antennas [6]. Besides, since IRS reflects signal passively in full-duplex mode without requiring any signal and noise amplification, it can be densely deployed and the spectral efficiency is much higher than conventional relaying and beamforming. Moreover, the feature of lightweight and low cost facilitates IRS scalable and adaptable deployment. Motivated by the above advantages, various IRS-assisted communication systems have been studied extensively, e.g., multiantenna system [7, 8], THz communication [9], integrated sensing and communication [10], radar communication [11], etc.

On the other hand, security is also a key issue in wireless communication. Traditional encryption technology relying on key distribution and management becomes very challenging in future hyper-connection networks. The application of computation-based cryptography techniques is restricted by the limited computing capability of terminal devices [12]. Fortunately, physical layer security exploiting the random nature of wireless channels offers low-complexity information theoretic-based security, which is viewed as a powerful complement to the existing security schemes. In recent years, IRS-aided PLS has been extensively studied in various fields, such as relay [13], MIMO [14], nonorthogonal multiple access [15], unmanned aerial vehicles networks [16, 17], THz communication [18], etc.

However, the majority of the existing researches focused on the beamforming design of single or noncooperative multiple IRSs [19, 20], which actually limits the potential of IRS for improving communication performance. Recently, cooperative double-IRS-assisted system has attracted much attentions. Different from single IRS and noncooperative double IRSs, each serving associated users independently, cooperative double IRS, which considering the inter-IRS channel, can bypass dense obstacles and further increase the network coverage, especially when the direct and two single-reflection links are all blocked [21]. Although the two-hop reflections in the double-IRS system incur an extra triple-path loss, it can be compensated by a sufficiently large number of IRS reflective elements and carefully selected deployment locations. The work [22] demonstrated that for a double-IRS-assisted SISO system with line-of-sight (LoS) inter-IRS channels, the cooperative beamforming scheme achieves $\mathcal{O}(M^4)$ power gain, while the system assisted by conventional single-IRS with equal number of reflection elements only yields $\mathcal{O}(M^2)$ power gain, given a sufficient total reflection elements M. Then, the work [23] analyzed the capacity scaling order in the MIMO network given the transmit power approaching infinity and shown that the performance achieved by cooperative double-IRS also significantly outperforms that of single-IRS. Motivated by these advantages, cooperative double IRS technology has been investigated in several applications. For instance, the work [24] investigated the multiuser (MU) MISO network assisted by double-IRS, where the fractional programing (FP) and block coordinate descent method were utilized to maximize the weight sum rate (WSR) of the system. Moreover, Zheng et al. [25] investigated the double-IRS-assisted uplink MIMO system and found that deploying two cooperative IRSs results in an increased rank of the channel matrix compared to deploying only one IRS. Then, the work [26] focused on a double-IRS-assisted MU-MIMO mmWave system, where the active beamforming at the base station (BS) and passive beamforming of IRSs are optimized by quadratically constrained quadratic programing (QCQP) and Riemannian manifold optimization, respectively. Also, in [27], a block minorization–maximization algorithm was proposed to maximize the WSR of a multi-RIS-assisted system. Lu et al. [28] considered the energy efficiency maximization of cooperative double-IRS-assisted MU-MIMO network where FP and semidefinite relaxation (SDR) were utilized to optimize the beamforming of BS and phase shifts of IRSs. For security issues, the work [29] proposed a double-IRS-assisted MISO secure system, where the product Riemmanian manifold optimization approach was developed to design the phase shift of IRSs.

From the above analysis, it is evident that there is a lack of sufficient research on cooperative double-IRS-aided PLS. Although a cooperative double-IRS-aided secure system was investigated, it only focused on the single-user scenario, leaving room for further investigation in MU scenarios. Besides, the incorporation of artificial noise (AN) can further enhance the secure performance [30, 31]. However, the joint design of AN and cooperative double-IRS in PLS is still in its infancy. Motivated by these observations, we investigate a novel MU-MISO secure network with multiple single-antenna noncolluding eavesdroppers. Specifically, two cooperative IRSs are deployed to enhance the secure performance of the network, and AN is emitted by the BS to deteriorate the wiretap channels. We summarize the main contributions of this paper as follows:

(1) We study the joint design of beamforming for transmitted signal and AN vector as well as the cooperative phase shifts of both IRSs in a double-IRS-aided MU-MISO secure communication system where the inter-IRS channel is considered. To evaluate the system performance, we establish the weighted sum secrecy rate (WSSR) maximization problem under the restrictions of transmit power budget and unit-module phase shift of IRS. Both continuous phase shift and discrete phase shift are considered in this work.

(2) The formulated problem is nonconvex due to the nonconcave objective function, the deeply coupled variables, and the unit-modulus constraint of IRS. To address this issue, we first derive an approximated concave lower bound of the objective function via a novel successive convex approximation (SCA) technique. Then, we propose a low-complexity alternating optimization (AO) algorithm to optimize each variable in an alternated manner. Specifically, transmit beamforming and AN vector are solved by using the Lagrange dual method and Karush–Kuhn–Tucker (KKT) conditions, while the phase shifts of the

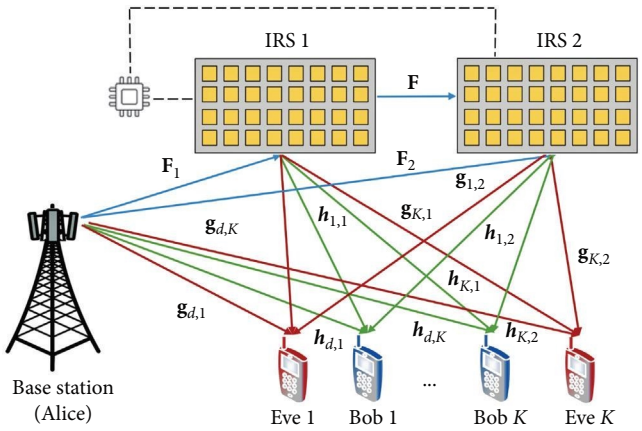

FIGURE 1: A cooperative double-IRS-aided MU-MISO downlink secure network.

cooperative IRSs are optimized by utilizing the alternating direction method of multipliers (ADMM).

(3) We demonstrate the convergence of the proposed algorithm through rigorous mathematical proof. Simulation results validate the advantage of employing cooperative double-IRS and the effectiveness of the proposed algorithm in practical implementation.

The rest of this paper is organized as follows: Section 2 introduces the considered cooperative double-IRS aided MU-MISO secure communication system and formulated a WSSR maximization problem. In Section 3, the proposed problem is solved by an AO algorithm. The proposed algorithm is evaluated by numerical results in Section 4, and conclusions are drawn in Section 5.

1.1. Notation. Boldface lower-case and boldface upper-case letters represent column vector and matrix, respectively. Superscript $(\cdot)^*$, $(\cdot)^{\mathrm{H}}$ and $(\cdot)^{\mathrm{T}}$ denotes the conjugate, transpose, and conjugated–transpose operation, respectively. The operators $\angle(\cdot)$, $|\cdot|$ and $\Re\{\cdot\}$, respectively, denote the angle, the absolute value, and the real part of a complex number. $\mathbb{E}\{\cdot\}$ denotes the statistical expectation. The notation $[\cdot]_n$ denotes the nth element of a vector. $j=\sqrt{-1}$ denote the imaginary unit, $[\cdot]^+ \triangleq \max(\cdot, 0)$.

2. System Model and Problem Formulation

As Figure 1 shows, we study a MU-MISO downlink secure broadcast network, which consists of a BS (Alice), two distributed IRSs (IRS 1 near BS and IRS 2 near users), K legitimated single-antenna users (Bobs) and K noncooperative single-antenna eavesdroppers (Eves). Alice is equipped with N transmit antennas while the number of passive reflective elements of IRS i is M_i with $i \in \{1, 2\}$. The smart controller equipped on each IRS is used to coordinate the information transmission and improve the secure performance of the system. It is assumed that all links experience quasi-static slow fading. The baseband equivalent channel coefficients from Alice to the IRS i, from IRS 1 to IRS 2, from Alice to the kth Bob/Eve, from IRS i to the kth Bob/Eve are denoted by $\mathbf{F}_i \in \mathbb{C}^{M_i \times N}$, $\mathbf{F} \in \mathbb{C}^{M_2 \times M_1}$, $\mathbf{h}_{d,k} \in \mathbb{C}^{N \times 1}$, $\mathbf{g}_{d,k} \in \mathbb{C}^{N \times 1}$, $\mathbf{h}_{k,i} \in \mathbb{C}^{M_i \times 1}$, $\mathbf{g}_{k,i} \in \mathbb{C}^{M_i \times 1}$ $(\forall i \in \{1, 2\}, \forall k \in \{1, \ldots, K\})$, respectively. The link of BS-IRS2-IRS1-Bobs/Eves is ignored due to the significant path loss [25]. In addition, it is assumed in this work that the channel state information (CSI) of all links is perfectly known to Alice and the IRSs, which allows us to consider the results obtained in this study as an upper bound for the secure performance of the system. Note that the assumption of perfect CSI of Eves is reasonable in the scenario where Eves are other system users but not trusted by Bobs [32]. In addition, the existing channel estimation technique in [33] can be utilized to estimate each channel. The direct channel between the BS and Bob/Eve is modeled as Rayleigh fading, while the other channel is assumed as Rician fading. Take $\mathbf{F}$ for example, which is given by the following:

$$\mathbf{F} = \sqrt{\frac{\kappa}{\kappa+1}}\mathbf{F}^{LoS} + \sqrt{\frac{1}{\kappa+1}}\mathbf{F}^{NLoS}, \tag{1}$$

where κ is the Ricean factor, $\mathbf{F}^{NLoS}$ and $\mathbf{F}^{LoS}$ denote the Rayleigh fading non-LoS component and the deterministic LoS component, respectively. Similar to [34], the IRSs are shaped as a uniform planar array with five horizontal elements. Thus $\mathbf{F}^{LoS}$ can be represented as $\mathbf{F}^{LoS} = \mathbf{a}_M(\mathbf{a}_N)^{\mathrm{H}}$, where $\mathbf{a}_N$ is the array response vectors of the receiver which modeled as follows:

$$\mathbf{a}_N(\nu, \psi) = \frac{1}{\sqrt{HV}}\Big[1, \ldots, e^{j2\pi\frac{d_e}{\lambda}(m\sin(\nu)\sin(\psi)+n\cos(\psi))} \ldots, e^{j2\pi\frac{d_e}{\lambda}((H-1)\sin(\nu)\sin(\psi)+(V-1)\cos(\psi))}\Big]^T, \tag{2}$$

where λ is the carrier wavelength, d_e is the separation between adjacent elements, ν and ψ, respectively, denote the azimuth angle and elevation angle of departure. $m \in [0, H]$ and $n \in [0, V]$ denote the horizontal and vertical element indices, respectively. The receive array response $\mathbf{a}_M$ can be defined similarly.

2.1. Signal Transmission Model. The BS sends K independent confidential data streams simultaneously to K Bobs. Meanwhile, K Eves distributed around Bobs attempt to wiretap the private information. Besides, AN is added to the transmitted signal to disrupt eavesdropping. Thus, the signal sent from the BS is given as $\mathbf{x} = \sum_{k=1}^{K}\mathbf{w}_k s_k + \mathbf{v}$, where $s_k \sim CN(0, 1)$ denotes the private message transmitted to the kth Bob with $\mathbb{E}\{|s_k|\} = 1$, $\mathbf{w}_k \in \mathbb{C}^{N \times 1}$ is the transmit beamforming vector and $\mathbf{v} \in \mathbb{C}^{N \times 1}$ denotes the AN which is assumed as a zero-mean circularly symmetric complex (ZMCSC) Gaussian vector, i.e., $\mathbf{v} \sim CN(0, \mathbf{V})$ where $\mathbf{V} \succeq 0$ denotes the covariance matrix. Therefore, the signal received at the kth Bob/Eve can be represented as follows:

$$y_{b,k} = \left(\mathbf{h}_{k,1}^{\mathrm{H}}\boldsymbol{\Phi}_1\mathbf{F}_1 + \mathbf{h}_{k,2}^{\mathrm{H}}\boldsymbol{\Phi}_2\mathbf{F}_2 + \mathbf{h}_{k,2}^{\mathrm{H}}\boldsymbol{\Phi}_2\mathbf{F}\boldsymbol{\Phi}_1\mathbf{F}_1 + \mathbf{h}_{d,k}^{\mathrm{H}}\right)\left(\sum_{k=1}^{K}\mathbf{w}_k s_k + \mathbf{v}\right) + n_{b,k}, \tag{3}$$

$$y_{e,k} = \left(\mathbf{g}_{k,1}^{\mathrm{H}}\boldsymbol{\Phi}_1\mathbf{F}_1 + \mathbf{g}_{k,2}^{\mathrm{H}}\boldsymbol{\Phi}_2\mathbf{F}_2 + \mathbf{g}_{k,2}^{\mathrm{H}}\boldsymbol{\Phi}_2\mathbf{F}\boldsymbol{\Phi}_1\mathbf{F}_1 + \mathbf{g}_{d,k}^{\mathrm{H}}\right)\left(\sum_{k=1}^{K}\mathbf{w}_k s_k + \mathbf{v}\right) + n_{e,k}, \tag{4}$$

respectively, where $\boldsymbol{\Phi}_i = \mathrm{diag}(\boldsymbol{\phi}_i)$, $\boldsymbol{\phi}_i = [e^{j\varphi_{i1}}, \ldots e^{j\varphi_{iM_i}}]$, $i \in [1, 2]$ denotes the phase shift matrix of IRS i. It should be noted that the amplitude of phase shift is assumed as a unit since the passive characteristic of IRS. $n_{b,k}$ and $n_{e,k}$, respectively, represent ZMCSC additive white Gaussian noise at the kth Bob/Eve, i.e., $n_{b,k} \sim CN(0, \sigma_{b,k}^2)$ and $n_{e,k} \sim CN(0, \sigma_{e,k}^2)$. For analytical purposes, it is assumed that each Eve, which is noncooperative with each other, solely attempts to wiretap their nearest Bob. Thus, the received signal-to-interference-plus-noise ratio at the kth Bob/Eve can be represented as follows [35]:

$$r_{b,k} = \frac{\left|\widehat{\mathbf{h}}_k^{\mathrm{H}}\mathbf{w}_k\right|^2}{\sum_{i=1,i\neq k}^{K}\left|\widehat{\mathbf{h}}_k^{\mathrm{H}}\mathbf{w}_i\right|^2 + \left|\widehat{\mathbf{h}}_k^{\mathrm{H}}\mathbf{v}\right|^2 + 1}, \tag{5}$$

$$r_{e,k} = \frac{\left|\widehat{\mathbf{g}}_k^{\mathrm{H}}\mathbf{w}_k\right|^2}{\sum_{i=1,i\neq k}^{K}\left|\widehat{\mathbf{g}}_k^{\mathrm{H}}\mathbf{w}_i\right|^2 + \left|\widehat{\mathbf{g}}_k^{\mathrm{H}}\mathbf{v}\right|^2 + 1}, \tag{6}$$

respectively, where $\widehat{\mathbf{h}}_k^{\mathrm{H}} = \mathbf{h}_k^{\mathrm{H}}/\sigma_{b,k}^2$, $\widehat{\mathbf{g}}_k^{\mathrm{H}} = \mathbf{g}_k^{\mathrm{H}}/\sigma_{e,k}^2$, $\mathbf{h}_k^{\mathrm{H}} = \mathbf{h}_{k,1}^{\mathrm{H}}\boldsymbol{\Phi}_1\mathbf{F}_1 + \mathbf{h}_{k,2}^{\mathrm{H}}\boldsymbol{\Phi}_2\mathbf{F}_2 + \mathbf{h}_{k,2}^{\mathrm{H}}\boldsymbol{\Phi}_2\mathbf{F}\boldsymbol{\Phi}_1\mathbf{F}_1 + \mathbf{h}_{d,k}^{\mathrm{H}}$, and $\mathbf{g}_k^{\mathrm{H}} = \mathbf{g}_{k,1}^{\mathrm{H}}\boldsymbol{\Phi}_1\mathbf{F}_1 + \mathbf{g}_{k,2}^{\mathrm{H}}\boldsymbol{\Phi}_2\mathbf{F}_2 + \mathbf{g}_{k,2}^{\mathrm{H}}\boldsymbol{\Phi}_2\mathbf{F}\boldsymbol{\Phi}_1\mathbf{F}_1 + \mathbf{g}_{d,k}^{\mathrm{H}}$. The achievable secrecy rate for the kth Bob can be written as follows:

$$R_{s,k} = \left[R_{b,k} - R_{e,k}\right]^+, \tag{7}$$

where $R_{b,k} = \ln(1 + r_{b,k})$ and $R_{e,k} = \ln(1 + r_{e,k})$ denote the achievable rate of kth Bob/Eve, respectively. To ensure simplicity in the subsequent sections of this paper, the operator $[\cdot]^+$ is omitted, given that the optimal secrecy rate cannot be negative [32].

2.2. Problem Formulation. In this work, we attempt to consider the maximization of the WSSR while satisfying the power budgets of the BS and the unit modulus constraints of IRS phase shifts. The WSSR is defined as $R_s \triangleq \sum_{k=1}^{K}\eta_k R_{s,k}$, where η_k denotes the nonnegative weight factor for the kth Bob. The considered optimization problem can be mathematically formulated as follows:

$$\max_{\mathbf{w}_k, \mathbf{v}, \boldsymbol{\phi}_1, \boldsymbol{\phi}_2} \quad R_s, \tag{8a}$$

$$\text{s.t.} \sum_{k=1}^{K}\|\mathbf{w}_k\|^2 + \|\mathbf{v}\|^2 \leq P_t^{\max}, \tag{8b}$$

$$|[\boldsymbol{\phi}_i]_m| = 1, \forall m \in \{1, \ldots M_i\}, i \in \{1, 2\}, \tag{8c}$$

where $P_t^{\max}$ denotes the transmit power budget at BS and constraint (8c) represents unit modulus phase shifts constraints. The optimal solution to problem (8) is challenging to find since the nonconcave objective function, the unit modulus constraint, and the highly coupled optimization variables.

3. The WSSR Maximization Algorithm Design

In this part, we first derive the approximated concave lower bound of R_s via a novel SCA technique. Then, we propose an AO algorithm to decompose the reformulated problem into three subproblems, i.e., optimizing $\{\mathbf{w}_k, \mathbf{v}\}$, $\boldsymbol{\phi}_1$, and $\boldsymbol{\phi}_2$, alternatively. To be specific, we adopt the Lagrange dual method and KKT condition to solve the subproblem with respect to $\{\mathbf{w}_k, \mathbf{v}\}$, where the optimal dual variable is found by using bisection method. The optimal phase shift $\boldsymbol{\phi}_i$ is iteratively derived by the ADMM method. At last, we extend the proposed algorithm to discrete phase shift cases. The convergence of the proposed algorithm is proved, and the computational complexity is analyzed.

3.1. Problem Transformation. To proceed, we derive an approximated lower bound of $R_{b,k}$ and an approximated upper bound of $R_{e,k}$ in Lemma 1.

Lemma 1. *The approximated lower bound of $R_{b,k}$ and the approximated upper bound of $R_{e,k}$ around a given point $\{\mathbf{w}_k^t, \mathbf{v}^t, \boldsymbol{\phi}_1^t, \boldsymbol{\phi}_2^t\}$ can be expressed as follows:*

$$R_{b,k} \geq \ln\left(1 + \frac{|x_k^t|^2}{y_k^t}\right) - \frac{|x_k^t|^2}{y_k^t} + \frac{2\Re\{(x_k^t)^* x_k\}}{y_k^t} - \frac{|x_k^t|^2(y_k + |x_k|^2)}{y_k^t(y_k^t + |x_k^t|^2)}, \tag{9}$$

$$R_{e,k} \leq \ln(1 + z_k^t) + \frac{1 + z_k}{1 + z_k^t} - 1 - \ln(1 + c_k^t) + c_k^t - 2\Re\{\mathbf{v}_i^{\mathrm{H}}\widehat{\mathbf{g}}_k(\widehat{\mathbf{g}}_k^{\mathrm{t}})^{\mathrm{H}}\mathbf{v}_i^t\} - 2\sum_{i=1,i\neq k}^{K}\Re\{\mathbf{w}_i^{\mathrm{H}}\widehat{\mathbf{g}}_k(\widehat{\mathbf{g}}_k^{\mathrm{t}})^{\mathrm{H}}\mathbf{w}_i^t\} + \frac{c_k^t}{1 + c_k^t}\left(1 + \sum_{i=1,i\neq k}^{K}\left|\widehat{\mathbf{g}}_k^{\mathrm{H}}\mathbf{w}_i\right|^2 + \left|\widehat{\mathbf{g}}_k^{\mathrm{H}}\mathbf{v}\right|^2\right), \tag{10}$$

where $x_k = \widehat{\mathbf{h}}_k^{\mathrm{H}}\mathbf{w}_k$, $x_k^t = \widehat{\mathbf{h}}_k^{\mathrm{H}}\mathbf{w}_k^t$, $y_k = 1 + \sum_{i=1,i\neq k}^{K}|\widehat{\mathbf{h}}_k^{\mathrm{H}}\mathbf{w}_i|^2 + |\widehat{\mathbf{h}}_k^{\mathrm{H}}\mathbf{v}|^2$, $y_k^t = 1 + \sum_{i=1,i\neq k}^{K}|\widehat{\mathbf{h}}_k^{\mathrm{H}}\mathbf{w}_i^t|^2 + |\widehat{\mathbf{h}}_k^{\mathrm{H}}\mathbf{v}^t|^2$, $z_k = \sum_{i=1}^{K}|\widehat{\mathbf{g}}_k^{\mathrm{H}}\mathbf{w}_i|^2 + |\widehat{\mathbf{g}}_k^{\mathrm{H}}\mathbf{v}|^2$, $z_k^t = \sum_{i=1}^{K}|\widehat{\mathbf{g}}_k^{\mathrm{H}}\mathbf{w}_i^t|^2 + |\widehat{\mathbf{g}}_k^{\mathrm{H}}\mathbf{v}^t|^2$, $c_k^t = \sum_{i=1,i\neq k}^{K}|\widehat{\mathbf{g}}_k^{\mathrm{H}}\mathbf{w}_i^t|^2 + |\widehat{\mathbf{g}}_k^{\mathrm{H}}\mathbf{v}^t|^2$.

Proof. Please see Appendix A.

The approximated lower bound for R_s can be obtained by subtracting Equations (9) and (10) to Equation (7). By neglecting the constant items, we obtain an equivalent formulation of problem (8), which is represented as follows:

$$\begin{aligned}\min_{\mathbf{w}_k,\mathbf{v},\phi_1,\phi_2}\ & \sum_{k=1}^{K}\eta_k\left\{\frac{c_k^t}{1+c_k^t}\left[\sum_{i=1,i\neq k}^{K}\left|\widehat{\mathbf{g}}_k^{\mathrm{H}}\mathbf{w}_i\right|^2+\left|\widehat{\mathbf{g}}_k^{\mathrm{H}}\mathbf{v}\right|^2\right]\right.\\ &+\frac{|x_k^t|^2\left(\sum_{i=1}^{K}\left|\widehat{\mathbf{h}}_k^{\mathrm{H}}\mathbf{w}_i\right|^2+\left|\widehat{\mathbf{h}}_k^{\mathrm{H}}\mathbf{v}\right|^2\right)}{y_k^t\left(y_k^t+|x_k^t|^2\right)}+\frac{\sum_{i=1}^{K}\left|\widehat{\mathbf{g}}_k^{\mathrm{H}}\mathbf{w}_i\right|^2+\left|\widehat{\mathbf{g}}_k^{\mathrm{H}}\mathbf{v}\right|^2}{1+z_k^t}\\ &-2\sum_{i=1,i\neq k}^{K}\Re\left\{\mathbf{w}_i^{\mathrm{H}}\widehat{\mathbf{g}}_k\left(\widehat{\mathbf{g}}_k^{\mathrm{t}}\right)^{\mathrm{H}}\mathbf{w}_i^t\right\}-2\Re\left\{\mathbf{v}^{\mathrm{H}}\widehat{\mathbf{g}}_k\left(\widehat{\mathbf{g}}_k^{\mathrm{t}}\right)^{\mathrm{H}}\mathbf{v}^t\right\}\\ &\left.-\frac{2\Re\left\{\mathbf{w}_k^{\mathrm{H}}\widehat{\mathbf{h}}_k\left(\widehat{\mathbf{h}}_k^t\right)^{\mathrm{H}}\mathbf{w}_k^t\right\}}{y_k^t}\right\},\end{aligned} \tag{11a}$$

$$\text{s.t. (8b)(8c).} \tag{11b}$$

However, the optimization variables in the reformulated problem are still highly coupled. To circumvent this issue, we adopt the AO technique to decouple these variables and optimize them in an alternated manner. □

3.2. Optimal Transmit Beamforming and AN Design. In this subsection, we optimize $\mathbf{w_k}$ and $\mathbf{v}$ with given ϕ_1 and ϕ_2. Let $\{\mathbf{w}_k^t,\mathbf{v}^t,\phi_1^t,\phi_2^t\}$ denotes a feasible point of problem (8) at the tth iteration. With some mathematical manipulations on the objective function (11), the problem (11) can be re-expressed as follows:

$$\min_{\mathbf{w}_k,\mathbf{v}}\ \sum_{k=1}^{K}\left(\mathbf{w}_k^{\mathrm{H}}\mathbf{A}_k\mathbf{w}_k-2\Re\left\{\mathbf{w}_k^{\mathrm{H}}\mathbf{b}_k\right\}\right)+\mathbf{v}^{\mathrm{H}}\widehat{\mathbf{A}}\mathbf{v}-2\Re\left\{\mathbf{v}^{\mathrm{H}}\widehat{\mathbf{b}}\right\}, \tag{12a}$$

$$\text{s.t. (8b)}, \tag{12b}$$

where

$$\begin{aligned}\mathbf{A}_k&=\eta_k\left(\frac{c_k^t}{1+c_k^t}\sum_{i=1,i\neq k}^{K}\widehat{\mathbf{g}}_i\widehat{\mathbf{g}}_i^{\mathrm{H}}+\frac{|x_k^t|^2\sum_{i=1}^{K}\widehat{\mathbf{h}}_i\widehat{\mathbf{h}}_i^{\mathrm{H}}}{y_k^t\left(y_k^t+|x_k^t|^2\right)}+\frac{\sum_{i=1}^{K}\widehat{\mathbf{g}}_i\widehat{\mathbf{g}}_i^{\mathrm{H}}}{1+z_k^t}\right)\\ \mathbf{b}_k&=\eta_k\left(\sum_{i=1,i\neq k}^{K}\widehat{\mathbf{g}}_i(\widehat{\mathbf{g}}_i^{\mathrm{t}})^{\mathrm{H}}\mathbf{w}_k^t+\frac{\widehat{\mathbf{h}}_k\left(\widehat{\mathbf{h}}_k^t\right)^{\mathrm{H}}\mathbf{w}_k^t}{y_k^t}\right)\\ \widehat{\mathbf{A}}&=\sum_{k=1}^{K}\eta_k\left(\frac{c_k^t}{1+c_k^t}\widehat{\mathbf{g}}_k\widehat{\mathbf{g}}_k^{\mathrm{H}}+\frac{|x_k^t|^2\widehat{\mathbf{h}}_k\widehat{\mathbf{h}}_k^{\mathrm{H}}}{y_k^t\left(y_k^t+|x_k^t|^2\right)}+\frac{\widehat{\mathbf{g}}_k\widehat{\mathbf{g}}_k^{\mathrm{H}}}{1+z_k^t}\right)\\ \widehat{\mathbf{b}}&=\sum_{k=1}^{K}\eta_k\widehat{\mathbf{g}}_k\left(\widehat{\mathbf{g}}_k^t\right)^{\mathrm{H}}\mathbf{v}^t.\end{aligned} \tag{13}$$

Problem (12) is QCQP, which can be solved by utilizing the CVX tool [36]. Here, we develop a low-complexity approach by using the Lagrange dual method and KKT conditions. First, we write the Lagrange function associated with Equation (12a) as follows:

$$\begin{aligned}\mathscr{L}(\mathbf{w}_k,\mathbf{v},\lambda)=&\sum_{k=1}^{K}\left(\mathbf{w}_k^{\mathrm{H}}\mathbf{A}_k\mathbf{w}_k-2\Re\left\{\mathbf{w}_k^{\mathrm{H}}\mathbf{b}_k\right\}\right)+\mathbf{v}^{\mathrm{H}}\widehat{\mathbf{A}}\mathbf{v}\\ &-2\Re\left\{\mathbf{v}^{\mathrm{H}}\widehat{\mathbf{b}}\right\}+\lambda\left(\sum_{k=1}^{K}\|\mathbf{w}_k\|^2+\|\mathbf{v}\|^2-P_t^{\max}\right),\end{aligned} \tag{14}$$

where $\lambda\geq 0$ is the Lagrange dual variable with respect to the constraint (8b). The corresponding dual problem is given by the following:

$$\min_{\mathbf{w}_k,\mathbf{v}}\ \mathscr{L}(\mathbf{w}_k,\mathbf{v},\lambda). \tag{15}$$

It is easy to proof that problem (12) is convex, leading to the assurance of strong duality between problem (12) and problem (15) based on Slater's condition. Therefore, the optimal solutions to problem (12) satisfy the following KKT conditions:

$$\frac{\partial\mathscr{L}\left(\mathbf{w}_k^*,\mathbf{v}^*,\lambda^*\right)}{\partial\mathbf{w}_k{}^*}=0, \tag{16a}$$

$$\frac{\partial\mathscr{L}\left(\mathbf{w}_k{}^*,\mathbf{v}^*,\lambda^*\right)}{\partial\mathbf{v}^*}=0, \tag{16b}$$

$$\lambda^*\left(\sum_{k=1}^{K}\|\mathbf{w}_k{}^*\|^2+\|\mathbf{v}^*\|^2-P_t^{\max}\right)=0. \tag{16c}$$

The optimal of problem (12) can be obtained by considering Equations (16a) and (16b) as follows:

$$\frac{\partial\mathscr{L}\left(\mathbf{w}_k^*,\mathbf{v}^*,\lambda^*\right)}{\partial\mathbf{w}_k^*}=0\Rightarrow\mathbf{w}_k^*(\lambda^*)=\Re\{\mathbf{b}_k\}(\mathbf{A}_k+\lambda^*\mathbf{I}_{N\times N})^{-1}, \tag{17a}$$

$$\frac{\partial\mathscr{L}\left(\mathbf{w}_k^*,\mathbf{v}^*,\lambda^*\right)}{\partial\mathbf{v}^*}=0\Rightarrow\mathbf{v}^*(\lambda^*)=\Re\left\{\widehat{\mathbf{b}}\right\}\left(\widehat{\mathbf{A}}+\lambda^*\mathbf{I}_{N\times N}\right)^{-1}. \tag{17b}$$

It is important to note that λ^* needs to satisfy Equation (16c); thus, the solution can be categorized into two situations: (1) If $\sum_{k=1}^{K}\|\mathbf{w}_k^*\|^2+\|\mathbf{v}^*\|^2\leq P_t^{\max}$ remains valid, then λ^* is set to 0. (2) Alternatively, λ^* can be determined by solving $\sum_{k=1}^{K}\|\mathbf{w}_k^*\|^2+\|\mathbf{v}^*\|^2=P_t^{\max}$. Recall that $\mathbf{w}_k^*$ and $\mathbf{v}^*$ satisfy Equations (17a) and (17b), respectively. Thus, the optimal λ^* can be obtained by adopting the bisection method. Based on the above discussion, the detailed steps for finding $(\mathbf{w}_k^*,\mathbf{v}^*,\lambda^*)$ are summarized in Algorithm 1.

3.3. Design of Phase Shift of IRS 1. In this part, we design the phase shift of IRS 1 with given $\{\mathbf{w}_k^t,\mathbf{v}^t,\phi_2^t\}$. We first recast $\mathbf{h}_k^{\mathrm{H}}$ and $\mathbf{g}_k^{\mathrm{H}}$ as follows:

1: **Initialization:** set the accuracy ϑ, a feasible point $\{\mathbf{w}^0, \mathbf{v}^0, \phi_1^0, \phi_2^0\}$ and the searching bounds λ^l and λ^u;
2: **Calculate** $\mathbf{w}_k^* = \Re\{\mathbf{b}_k\}\mathbf{A}_k^{-1}$ and $\mathbf{v}^* = \Re\{\widehat{\mathbf{b}}\}\widehat{\mathbf{A}}^{-1}$. **If** $\sum_{k=1}^K \|\mathbf{w}_k{}^*\|^2 + \|\mathbf{v}^*\|^2 \le P_t^{\max}$ **then** $\lambda^* = 0$ and **terminate**; **Otherwise**, move to step 3;
3: **Repeat**
4: **Calculate** $\lambda^* = (\lambda^l + \lambda^u)/2$;
5: **Update** $\mathbf{w}_k^*$ and $\mathbf{v}^*$ according to Equations (17a) and (17b), respectively;
6: **If** $\sum_{k=1}^K \|\mathbf{w}_k{}^*\|^2 + \|\mathbf{v}^*\|^2 \le P_t^{\max}$ **set** $\lambda^l = \lambda^*$; **Otherwise**, **set** $\lambda^u = \lambda^*$ **end if**;
7: **Until** $|\lambda^l - \lambda^u| \le \vartheta$;
8: **Output** $\{\mathbf{w}_k{}^*, \mathbf{v}^*, \lambda^*\}$.

Algorithm 1: Lagrange dual algorithm for problem (12).

$$\begin{aligned}\mathbf{h}_k^{\mathrm{H}} &= \mathbf{h}_{k,1}^{\mathrm{H}}\boldsymbol{\Phi}_1\mathbf{F}_1 + \mathbf{h}_{k,2}^{\mathrm{H}}\boldsymbol{\Phi}_2\mathbf{F}_2 + \mathbf{h}_{k,2}^{\mathrm{H}}\boldsymbol{\Phi}_2\mathbf{F}\boldsymbol{\Phi}_1\mathbf{F}_1 + \mathbf{h}_{d,k}^{\mathrm{H}} \\ &= \phi_1^{\mathrm{H}}\mathrm{diag}\left(\mathbf{h}_{k,1}^{\mathrm{H}}\right)\mathbf{F}_1 + \phi_2^{\mathrm{H}}\mathrm{diag}\left(\mathbf{h}_{k,2}^{\mathrm{H}}\right)\mathbf{F}_2 \\ &\quad + \phi_1^{\mathrm{H}}\mathrm{diag}\left(\phi_2^{\mathrm{H}}\mathrm{diag}\left(\mathbf{h}_{k,2}^{\mathrm{H}}\right)\mathbf{F}\right)\mathbf{F}_1 + \mathbf{h}_{d,k}^{\mathrm{H}} \\ &= \phi_1^{\mathrm{H}}\left(\mathrm{diag}\left(\mathbf{h}_{k,1}^{\mathrm{H}}\right)\mathbf{F}_1 + \mathrm{diag}\left(\phi_2^{\mathrm{H}}\mathrm{diag}\left(\mathbf{h}_{k,2}^{\mathrm{H}}\right)\mathbf{F}\right)\mathbf{F}_1\right) \\ &\quad + \phi_2^{\mathrm{H}}\mathrm{diag}\left(\mathbf{h}_{k,2}^{\mathrm{H}}\right)\mathbf{F}_2 + \mathbf{h}_{d,k}^{\mathrm{H}} \\ &= \widehat{\phi}_1^{\mathrm{H}}\mathbf{H}_k,\end{aligned} \tag{18}$$

$$\begin{aligned}\mathbf{g}_k^{\mathrm{H}} &= \mathbf{g}_{k,1}^{\mathrm{H}}\boldsymbol{\Phi}_1\mathbf{F}_1 + \mathbf{g}_{k,2}^{\mathrm{H}}\boldsymbol{\Phi}_2\mathbf{F}_2 + \mathbf{g}_{k,2}^{\mathrm{H}}\boldsymbol{\Phi}_2\mathbf{F}\boldsymbol{\Phi}_1\mathbf{F}_1 + \mathbf{g}_{d,k}^{\mathrm{H}} \\ &= \phi_1^{\mathrm{H}}\mathrm{diag}\left(\mathbf{g}_{k,1}^{\mathrm{H}}\right)\mathbf{F}_1 + \phi_2^{\mathrm{H}}\mathrm{diag}\left(\mathbf{g}_{k,2}^{\mathrm{H}}\right)\mathbf{F}_2 \\ &\quad + \phi_1^{\mathrm{H}}\mathrm{diag}\left(\phi_2^{\mathrm{H}}\mathrm{diag}\left(\mathbf{g}_{k,2}^{\mathrm{H}}\right)\mathbf{F}\right)\mathbf{F}_1 + \mathbf{g}_{d,k}^{\mathrm{H}} \\ &= \phi_1^{\mathrm{H}}\left(\mathrm{diag}\left(\mathbf{g}_{k,1}^{\mathrm{H}}\right)\mathbf{F}_1 + \mathrm{diag}\left(\phi_2^{\mathrm{H}}\mathrm{diag}\left(\mathbf{g}_{k,2}^{\mathrm{H}}\right)\mathbf{F}\right)\mathbf{F}_1\right) \\ &\quad + \phi_2^{\mathrm{H}}\mathrm{diag}\left(\mathbf{g}_{k,2}^{\mathrm{H}}\right)\mathbf{F}_2 + \mathbf{g}_{d,k}^{\mathrm{H}} \\ &= \widehat{\phi}_1^{\mathrm{H}}\mathbf{G}_k,\end{aligned} \tag{19}$$

where $\widehat{\phi}_1 = [\phi_1^{\mathrm{H}}, 1]^{\mathrm{H}}$ and

$$\begin{aligned}\mathbf{H}_k = &\left[\mathrm{diag}\left(\mathbf{h}_{k,1}^{\mathrm{H}}\right)\mathbf{F}_1 + \mathrm{diag}\left(\phi_2^{\mathrm{H}}\mathrm{diag}\left(\mathbf{h}_{k,2}^{\mathrm{H}}\right)\mathbf{F}\right)\mathbf{F}_1\right. \\ &\left.\phi_2^{\mathrm{H}}\mathrm{diag}\left(\mathbf{h}_{k,2}^{\mathrm{H}}\right)\mathbf{F}_2 + \mathbf{h}_{d,k}^{\mathrm{H}}\right]^{\mathrm{T}},\end{aligned} \tag{20a}$$

$$\begin{aligned}\mathbf{G}_k = &\left[\mathrm{diag}\left(\mathbf{g}_{k,1}^{\mathrm{H}}\right)\mathbf{F}_1 + \mathrm{diag}\left(\phi_2^{\mathrm{H}}\mathrm{diag}\left(\mathbf{g}_{k,2}^{\mathrm{H}}\right)\mathbf{F}\right)\mathbf{F}_1\right. \\ &\left.\phi_2^{\mathrm{H}}\mathrm{diag}\left(\mathbf{g}_{k,2}^{\mathrm{H}}\right)\mathbf{F}_2 + \mathbf{g}_{d,k}^{\mathrm{H}}\right]^{\mathrm{T}}.\end{aligned} \tag{20b}$$

Let $\widehat{\mathbf{H}}_k = \mathbf{H}_k/\sigma_{b,k}$ and $\widehat{\mathbf{G}}_k = \mathbf{G}_k/\sigma_{e,k}$, we can, respectively, represent $\widehat{\mathbf{h}}_k^{\mathrm{H}}$ and $\widehat{\mathbf{g}}_k^{\mathrm{H}}$ as follows:

$$\widehat{\mathbf{h}}_k^{\mathrm{H}} = \widehat{\phi}_1^{\mathrm{H}}\widehat{\mathbf{H}}_k, \tag{21a}$$

$$\widehat{\mathbf{g}}_k^{\mathrm{H}} = \widehat{\phi}_1^{\mathrm{H}}\mathbf{G}_k. \tag{21b}$$

By substituting Equations (21a) and (21b) into Equation (11), it is readily to formulate an optimization problem w.r.t. $\widehat{\phi}_1$.

$$\begin{aligned}\min_{\widehat{\phi}_1} \sum_{k=1}^K\ & \eta_k\left\{\frac{c_k^t}{1+c_k^t}\left[\sum_{i=1,i\neq k}^K\left|\widehat{\phi}_1^{\mathrm{H}}\widehat{\mathbf{G}}_k\mathbf{w}_i\right|^2 + \left|\widehat{\phi}_1^{\mathrm{H}}\widehat{\mathbf{G}}_k\mathbf{v}\right|^2\right]\right. \\ &+\frac{|x_k^t|^2\left(\sum_{i=1}^K\left|\widehat{\phi}_1^{\mathrm{H}}\widehat{\mathbf{H}}_k\mathbf{w}_i\right|^2 + \left|\widehat{\phi}_1^{\mathrm{H}}\widehat{\mathbf{H}}_k\mathbf{v}\right|^2\right)}{y_k^t\left(y_k^t + |x_k^t|^2\right)} \\ &+\frac{\sum_{i=1}^K\left|\widehat{\phi}_1^{\mathrm{H}}\widehat{\mathbf{G}}_k\mathbf{w}_i\right|^2 + \left|\widehat{\phi}_1^{\mathrm{H}}\widehat{\mathbf{G}}_k\mathbf{v}\right|^2}{1+z_k^t} \\ &-2\sum_{i=1,i\neq k}^K\Re\left\{(\mathbf{w}_i)^{\mathrm{H}}\widehat{\mathbf{G}}_k^{\mathrm{H}}\widehat{\phi}_1\left(\widehat{\phi}_1^t\right)^{\mathrm{H}}\widehat{\mathbf{G}}_k\mathbf{w}_i^t\right\} \\ &-2\Re\left\{(\mathbf{v}_i)^{\mathrm{H}}\widehat{\mathbf{G}}_k^{\mathrm{H}}\widehat{\phi}_1\left(\widehat{\phi}_1^t\right)^{\mathrm{H}}\widehat{\mathbf{G}}_k\mathbf{v}_i^t\right\} \\ &\left.-\frac{2\Re\left\{(\mathbf{w}_k)^{\mathrm{H}}\widehat{\mathbf{H}}_k^{\mathrm{H}}\widehat{\phi}_1\left(\widehat{\phi}_1^t\right)^{\mathrm{H}}\widehat{\mathbf{H}}_k\mathbf{w}_k^t\right\}}{y_k^t}\right\},\end{aligned} \tag{22a}$$

$$\text{s.t. } \left|\left[\widehat{\phi}_1\right]_m\right| = 1, \forall m \in \{1, \ldots M_1\}, \left[\widehat{\phi}_1\right]_{M_1+1} = 1. \tag{22b}$$

To proceed, we reform the problem (22) into the following quadratic problem:

$$\min_{\widehat{\phi}_1} \widehat{\phi}_1^{\mathrm{H}}\Omega\widehat{\phi}_1 - 2\Re\left\{\widehat{\phi}_1^{\mathrm{H}}\varphi\right\}, \tag{23a}$$

$$\text{s.t. } \left|\left[\widehat{\phi}_1\right]_m\right| = 1, \forall m \in \{1, \ldots M_1\}, \left[\widehat{\phi}_1\right]_{M_1+1} = 1, \tag{23b}$$

where $\Omega = \sum_{k=1}^K \eta_k\Omega_k$ and $\varphi = \sum_{k=1}^K \eta_k\varphi_k$. Ω_k and φ_k are, respectively, denoted as follows:

$$\begin{aligned}\Omega_k = &\frac{\left|x_k^t\right|^2\widehat{\mathbf{H}}_k\left(\sum_{i=1}^{K}\mathbf{w}_i^t(\mathbf{w}_i^t)^{\mathrm{H}}+\mathbf{v}^t(\mathbf{v}^t)^{\mathrm{H}}\right)\widehat{\mathbf{H}}_k^{\mathrm{H}}}{y_k^t\left(y_k^t+\left|x_k^t\right|^2\right)}\\ &+\frac{\widehat{\mathbf{G}}_k\left(\sum_{i=1}^{K}\mathbf{w}_i^t(\mathbf{w}_i^t)^{\mathrm{H}}+\mathbf{v}^t(\mathbf{v}^t)^{\mathrm{H}}\right)\widehat{\mathbf{G}}_k^{\mathrm{H}}}{1+z_k^t}\\ &+\frac{c_k^t\widehat{\mathbf{G}}_k\left(\sum_{i=1,i\neq k}^{K}\mathbf{w}_i^t(\mathbf{w}_i^t)^{\mathrm{H}}+\mathbf{v}^t(\mathbf{v}^t)^{\mathrm{H}}\right)\widehat{\mathbf{G}}_k^{\mathrm{H}}}{1+c_k^t},\end{aligned} \tag{24a}$$

$$\begin{aligned}\varphi_k = &\frac{\widehat{\mathbf{H}}_k\mathbf{w}_k^t\left(\mathbf{w}_k^t\right)^{\mathrm{H}}\widehat{\mathbf{h}}_k^{\mathrm{H}}\widehat{\boldsymbol{\phi}}_1^t}{y_k^t}\\ &+\widehat{\mathbf{g}}_k\left(\sum_{i=1,i\neq k}^{K}\mathbf{w}_i^t(\mathbf{w}_i^t)^{\mathrm{H}}+\mathbf{v}^t(\mathbf{v}^t)^{\mathrm{H}}\right)\widehat{\mathbf{G}}_k^{\mathrm{H}}\widehat{\boldsymbol{\phi}}_1^t.\end{aligned} \tag{24b}$$

Problem (23) can be solved by adopting SDR and Gaussian randomization method with the computational complexity of $\mathcal{O}((M_1+1)^2)$ [37]. Here, we propose a low complexity algorithm based on the ADMM method to iteratively derive the suboptimal solution of $\widehat{\boldsymbol{\phi}}_1$.

The basic idea of the ADMM method is to decompose a complex problem into more manageable subproblems and solve them iteratively. According to the ADMM method, we first introduce a slack variable $\mathbf{a}$, satisfying $\mathbf{a}=\widehat{\boldsymbol{\phi}}_1$, to problem (23) and reformulate it as follows:

$$\min_{\mathbf{a},\widehat{\boldsymbol{\phi}}_1}\ \mathbf{a}^{\mathrm{H}}\Omega\mathbf{a}-2\Re\{\mathbf{a}^{\mathrm{H}}\varphi\}, \tag{25a}$$

$$\text{s.t. }\left|\left[\widehat{\boldsymbol{\phi}}_1\right]_m\right|=1,\forall m\in\{1,\dots M_1\},\left[\widehat{\boldsymbol{\phi}}_1\right]_{M_1+1}=1, \tag{25b}$$

$$\mathbf{a}=\widehat{\boldsymbol{\phi}}_1. \tag{25c}$$

Then, we write the augmented Lagrange dual function of Equation (25) as follows:

$$\begin{aligned}\mathscr{L}\left(\mathbf{a},\widehat{\boldsymbol{\phi}}_1,\mathbf{d}\right)=&\mathbf{a}^{\mathrm{H}}\Omega\mathbf{a}-2\Re\{\mathbf{a}^{\mathrm{H}}\varphi\}-\Re\left\{\mathbf{d}^{\mathrm{H}}\left(\mathbf{a}-\widehat{\boldsymbol{\phi}}_1\right)\right\}\\ &+\frac{\tau}{2}\left\|\mathbf{a}-\widehat{\boldsymbol{\phi}}_1\right\|^2,\end{aligned} \tag{26}$$

where $\mathbf{d}\in\mathbb{C}^{N\times 1}$ is the Lagrange dual vector regarding constraint (25c) and $\tau\geq 0$ is the penalty factor. To proceed, we update variables $\mathbf{a}$, $\widehat{\boldsymbol{\phi}}_1$ and $\mathbf{d}$ iteratively by following the steps of ADMM framework. We denote the feasible solutions at the ith iteration as $\mathbf{a}^i$, $\widehat{\boldsymbol{\phi}}_1^i$ and $\mathbf{d}^i$, and calculate $\mathbf{a}^{i+1}$, $\widehat{\boldsymbol{\phi}}_1^{i+1}$ and $\mathbf{d}^{i+1}$ by sequentially solving the following subproblems:

(1) The subproblem associated with updating $\mathbf{a}^{i+1}$ is given by the following:

$$\mathbf{a}^{i+1}=\arg\min_{\mathbf{a}}\ \mathscr{L}\left(\mathbf{a},\widehat{\boldsymbol{\phi}}_1^i,\mathbf{d}^i\right). \tag{27}$$

Problem (27) can be solved by utilizing the first-order optimality condition of Equation (26), i.e.,

$$2\Omega\mathbf{a}^{i+1}-2\varphi-\mathbf{d}^i-\tau\left(\mathbf{a}^{i+1}-\widehat{\boldsymbol{\phi}}_1^i\right)=0. \tag{28}$$

After performing a few mathematical manipulations to Equation (28), we obtain $\mathbf{a}^{i+1}$ as follows:

$$\mathbf{a}^{i+1}=(\tau\mathbf{I}+2\Omega)^{-1}\left(2\varphi+\tau\widehat{\boldsymbol{\phi}}_1^i+\mathbf{d}^i\right). \tag{29}$$

(2) To obtain $\widehat{\boldsymbol{\phi}}_1^{i+1}$, the following subproblem needs to be solved:

$$\widehat{\boldsymbol{\phi}}_1^{i+1}=\arg\min_{\widehat{\boldsymbol{\phi}}_1^i}\ \mathscr{L}\left(\mathbf{a}^{i+1},\widehat{\boldsymbol{\phi}}_1^i,\mathbf{d}^i\right), \tag{30}$$

which is equivalent to the subsequent projection problem

$$\min_{\widehat{\boldsymbol{\phi}}_1}\ \left\|\widehat{\boldsymbol{\phi}}_1-\left(\mathbf{a}^{k+1}-\tau^{-1}\mathbf{d}^k\right)\right\|^2,\text{ s.t. (22b).} \tag{31}$$

Thus, the corresponding solution can be derived as follows:

$$\left[\widehat{\boldsymbol{\phi}}_1^{i+1}\right]_{\mathrm{m}}=\begin{cases}\dfrac{\left[\mathbf{r}^{i+1}-\tau^{-1}\mathbf{p}^i\right]_m}{\left|\left[\mathbf{r}^{i+1}-\tau^{-1}\mathbf{p}^i\right]_m\right|}, & \text{if}\left[\mathbf{r}^{i+1}-\tau^{-1}\mathbf{p}^i\right]_m\neq 0\\ \left[\widehat{\boldsymbol{\phi}}_1^i\right]_{\mathrm{m}}, & \text{otherwise}\end{cases}\quad\forall m\in\{1,\dots M_1\}. \tag{32}$$

(3) $\mathbf{d}^{k+1}$ can be obtained by employing the following equality:

$$\mathbf{d}^{i+1}=\mathbf{d}^i-\tau\left(\mathbf{a}^{i+1}-\widehat{\boldsymbol{\phi}}_1^{i+1}\right). \tag{33}$$

By substituting Equation (28) into Equation (34), we derive the $\mathbf{d}^{k+1}$ as follows:

$$\mathbf{d}^{k+1}=2\mathbf{A}\mathbf{a}^{k+1}-2\varphi. \tag{34}$$

The convergence of the ADMM algorithm is guaranteed when the value of penalty factor τ satisfies: $\tau\mathbf{I}/2-\mathbf{A}\succ 0$ [38].

1: **Initialization:** $i=0$, set the accuracy ϑ, set initial points $\{\mathbf{w}_k^0, \mathbf{v}^0, \widehat{\phi}_1^0, \widehat{\phi}_2^0\}$ and the maximum iteration number L;
2: **Set** penalty factor $\tau=\rho\|\mathbf{A}\|$ where ρ is the minimum integer satisfying $\tau\mathbf{I}/2 - \mathbf{A}\succ 0$;
3: **Repeat** i
4: **Obtain** $\mathbf{a}^{i+1}$ according to Equation (29);
5: **Obtain** $\widehat{\phi}_1^{i+1}$ according to Equation (32);
6: **Obtain** $\mathbf{d}^{i+1}$ according to Equation (34);
7: **Until** $|R_s(\widehat{\phi}_1^{i+1}) - R_s(\widehat{\phi}_1^{i})| \Big/ R_s(\widehat{\phi}_1^{i+1}) \le \vartheta$ or $i>L$;
8: **Output** $\widehat{\phi}_1^{*}$.

Algorithm 2: The ADMM algorithm for problem (22).

The overall procedures of the ADMM algorithm to solve problem (23) are listed in Algorithm 2.

3.4. Design of Phase Shift of IRS 2. In this subsection, we aim to solve the subproblem in terms of ϕ_2 with given $\{\mathbf{w}_k^t, \mathbf{v}^t, \phi_1^t\}$. Let us recast $\mathbf{h}_k^{\mathrm{H}}$ and $\mathbf{g}_k^{\mathrm{H}}$ as follows,

$$\begin{aligned}\mathbf{h}_k^{\mathrm{H}} &= \mathbf{h}_{k,1}^{\mathrm{H}}\boldsymbol{\Phi}_1\mathbf{F}_1 + \mathbf{h}_{k,2}^{\mathrm{H}}\boldsymbol{\Phi}_2\mathbf{F}_2 + \mathbf{h}_{k,2}^{\mathrm{H}}\boldsymbol{\Phi}_2\mathbf{F}\boldsymbol{\Phi}_1\mathbf{F}_1 + \mathbf{h}_{d,k}^{\mathrm{H}}\\ &= \boldsymbol{\phi}_1^{\mathrm{H}}\mathrm{diag}\left(\mathbf{h}_{k,1}^{\mathrm{H}}\right)\mathbf{F}_1 + \boldsymbol{\phi}_2^{\mathrm{H}}\mathrm{diag}\left(\mathbf{h}_{k,2}^{\mathrm{H}}\right)\mathbf{F}_2\\ &\quad + \boldsymbol{\phi}_2^{\mathrm{H}}\mathrm{diag}\left(\mathbf{h}_{k,2}^{\mathrm{H}}\right)\mathbf{F}\boldsymbol{\Phi}_1\mathbf{F}_1 + \mathbf{h}_{d,k}^{\mathrm{H}}\\ &= \boldsymbol{\phi}_2^{\mathrm{H}}\left(\mathrm{diag}\left(\mathbf{h}_{k,2}^{\mathrm{H}}\right)\mathbf{F}_2 + \mathrm{diag}\left(\mathbf{h}_{k,2}^{\mathrm{H}}\right)\mathbf{F}\boldsymbol{\Phi}_1\mathbf{F}_1\right)\\ &\quad + \boldsymbol{\phi}_1^{\mathrm{H}}\mathrm{diag}\left(\mathbf{h}_{k,1}^{\mathrm{H}}\right)\mathbf{F}_1 + \mathbf{h}_{d,k}^{\mathrm{H}}\\ &= \widehat{\boldsymbol{\phi}}_2^{\mathrm{H}}\breve{\mathbf{H}}_k,\end{aligned} \tag{35}$$

$$\begin{aligned}\mathbf{g}_k^{\mathrm{H}} &= \mathbf{g}_{k,1}^{\mathrm{H}}\boldsymbol{\Phi}_1\mathbf{F}_1 + \mathbf{g}_{k,2}^{\mathrm{H}}\boldsymbol{\Phi}_2\mathbf{F}_2 + \mathbf{g}_{k,2}^{\mathrm{H}}\boldsymbol{\Phi}_2\mathbf{F}\boldsymbol{\Phi}_1\mathbf{F}_1 + \mathbf{g}_{d,k}^{\mathrm{H}}\\ &= \boldsymbol{\phi}_1^{\mathrm{H}}\mathrm{diag}\left(\mathbf{g}_{k,1}^{\mathrm{H}}\right)\mathbf{F}_1 + \boldsymbol{\phi}_2^{\mathrm{H}}\mathrm{diag}\left(\mathbf{g}_{k,2}^{\mathrm{H}}\right)\mathbf{F}_2\\ &\quad + \boldsymbol{\phi}_2^{\mathrm{H}}\mathrm{diag}\left(\mathbf{g}_{k,2}^{\mathrm{H}}\right)\mathbf{F}\boldsymbol{\Phi}_1\mathbf{F}_1 + \mathbf{g}_{d,k}^{\mathrm{H}}\\ &= \boldsymbol{\phi}_2^{\mathrm{H}}\left(\mathrm{diag}\left(\mathbf{g}_{k,2}^{\mathrm{H}}\right)\mathbf{F}_2 + \mathrm{diag}\left(\mathbf{g}_{k,2}^{\mathrm{H}}\right)\mathbf{F}\boldsymbol{\Phi}_1\mathbf{F}_1\right)\\ &\quad + \boldsymbol{\phi}_1^{\mathrm{H}}\mathrm{diag}\left(\mathbf{g}_{k,1}^{\mathrm{H}}\right)\mathbf{F}_1 + \mathbf{g}_{d,k}^{\mathrm{H}}\\ &= \widehat{\boldsymbol{\phi}}_2^{\mathrm{H}}\breve{\mathbf{G}}_k,\end{aligned} \tag{36}$$

where $\widehat{\boldsymbol{\phi}}_2 = [\boldsymbol{\phi}_2^{\mathrm{H}}, 1]^{\mathrm{H}}$ and

$$\begin{aligned}\breve{\mathbf{H}}_k = \Big[&\mathrm{diag}\left(\mathbf{h}_{k,2}^{\mathrm{H}}\right)\mathbf{F}_2 + \mathrm{diag}\left(\mathbf{h}_{k,2}^{\mathrm{H}}\right)\mathbf{F}\boldsymbol{\Phi}_1\mathbf{F}_1\\ &\boldsymbol{\phi}_1^{\mathrm{H}}\mathrm{diag}\left(\mathbf{h}_{k,1}^{\mathrm{H}}\right)\mathbf{F}_1 + \mathbf{h}_{d,k}^{\mathrm{H}}\Big]^{\mathrm{T}},\end{aligned} \tag{37a}$$

$$\begin{aligned}\breve{\mathbf{G}}_k = \Big[&\mathrm{diag}\left(\mathbf{g}_{k,2}^{\mathrm{H}}\right)\mathbf{F}_2 + \mathrm{diag}\left(\mathbf{g}_{k,2}^{\mathrm{H}}\right)\mathbf{F}\boldsymbol{\Phi}_1\mathbf{F}_1\\ &\boldsymbol{\phi}_1^{\mathrm{H}}\mathrm{diag}\left(\mathbf{g}_{k,1}^{\mathrm{H}}\right)\mathbf{F}_1 + \mathbf{g}_{d,k}^{\mathrm{H}}\Big]^{\mathrm{T}}.\end{aligned} \tag{37b}$$

Let $\tilde{\mathbf{H}}_k = \breve{\mathbf{H}}_k/\sigma_{b,k}$ and $\tilde{\mathbf{G}}_k = \breve{\mathbf{G}}_k/\sigma_{e,k}$, we have the following:

$$\widehat{\mathbf{h}}_k^{\mathrm{H}} = \widehat{\boldsymbol{\phi}}_2^{\mathrm{H}}\widetilde{\mathbf{H}}_k, \tag{38a}$$

$$\widehat{\mathbf{g}}_k^{\mathrm{H}} = \widehat{\boldsymbol{\phi}}_2^{\mathrm{H}}\widetilde{\mathbf{G}}_k. \tag{38b}$$

By substituting Equations (38a) and (38b) into Equation (11) and following similar steps as in the previous subsection, the problem w.r.t $\widehat{\boldsymbol{\phi}}_2$ is formulated as follows:

$$\min_{\widehat{\boldsymbol{\phi}}_2}\ \widehat{\boldsymbol{\phi}}_2^{\mathrm{H}}\widehat{\boldsymbol{\Omega}}\widehat{\boldsymbol{\phi}}_2 - 2\Re\left\{\widehat{\boldsymbol{\phi}}_2^{\mathrm{H}}\widehat{\boldsymbol{\varphi}}\right\}, \tag{39a}$$

$$\text{s.t.}\ \left|\left[\widehat{\boldsymbol{\phi}}_2\right]_m\right| = 1, \forall m \in \{1, \ldots M_2\}, \left[\widehat{\boldsymbol{\phi}}_1\right]_{M_2+1} = 1, \tag{39b}$$

where $\widehat{\boldsymbol{\Omega}} = \sum_{k=1}^{K}\eta_k\widehat{\boldsymbol{\Omega}}_k$ and $\widehat{\boldsymbol{\varphi}} = \sum_{k=1}^{K}\eta_k\widehat{\boldsymbol{\varphi}}_k$. $\widehat{\boldsymbol{\Omega}}$ and $\widehat{\boldsymbol{\varphi}}$ are, respectively, denoted as follows:

$$\begin{aligned}\widehat{\boldsymbol{\Omega}}_k = &\frac{|x_k^t|^2\widetilde{\mathbf{H}}_k\left(\sum_{i=1}^{K}\mathbf{w}_i^t(\mathbf{w}_i^t)^{\mathrm{H}} + \mathbf{v}^t(\mathbf{v}^t)^{\mathrm{H}}\right)\widetilde{\mathbf{H}}_k^{\mathrm{H}}}{y_k^t\left(y_k^t + |x_k^t|^2\right)}\\ &+ \frac{\widetilde{\mathbf{G}}_k\left(\sum_{i=1}^{K}\mathbf{w}_i^t(\mathbf{w}_i^t)^{\mathrm{H}} + \mathbf{v}^t(\mathbf{v}^t)^{\mathrm{H}}\right)\widetilde{\mathbf{G}}_k^{\mathrm{H}}}{1+z_k^t}\\ &+ \frac{c_k^t\widetilde{\mathbf{G}}_k\left(\sum_{i=1,i\neq k}^{K}\mathbf{w}_i^t(\mathbf{w}_i^t)^{\mathrm{H}} + \mathbf{v}^t(\mathbf{v}^t)^{\mathrm{H}}\right)\widetilde{\mathbf{G}}_k^{\mathrm{H}}}{1+c_k^t},\end{aligned} \tag{40a}$$

$$\begin{aligned}\widehat{\boldsymbol{\varphi}}_k = &\frac{\widetilde{\mathbf{H}}_k\mathbf{w}_k^t(\mathbf{w}_k^t)^{\mathrm{H}}\widetilde{\mathbf{H}}_k^{\mathrm{H}}\widehat{\boldsymbol{\phi}}_2^t}{y_k^t}\\ &+ \widetilde{\mathbf{G}}_k\left(\sum_{i=1,i\neq k}^{K}\mathbf{w}_i^t(\mathbf{w}_i^t)^{\mathrm{H}} + \mathbf{v}^t(\mathbf{v}^t)^{\mathrm{H}}\right)\widetilde{\mathbf{G}}_k^{\mathrm{H}}\widehat{\boldsymbol{\phi}}_2^t.\end{aligned} \tag{40b}$$

The problem (39) can be solved by applying the ADMM method as described in the previous subsection, which is omitted for space saving.

Based on the above discussions, we summarize the AO algorithm, which updating each variable iteratively in Algorithm 3, where R_s^{i+1} represents the WSSR obtained at the ith iteration.

1: **Initialization:** set the accuracy ε, a feasible point $\{\mathbf{w}_k^0, \mathbf{v}^0, \phi_1^0, \phi_2^0\}$ and the maximum iteration number L, calculate R_s^0;
2: **Repeat** i
3: **Update** $\mathbf{w}_k^{i+1}$ and $\mathbf{v}^{i+1}$ by solving problem (12) with given $\{\mathbf{w}_k^i, \mathbf{v}^i, \phi_1^i, \phi_2^i\}$;
4: **Update** ϕ_1^{i+1} by solving problem (23) with given $\{\mathbf{w}_k^{i+1}, \mathbf{v}^{i+1}, \phi_1^i, \phi_2^i\}$;
5: **Update** ϕ_2^{i+1} by solving problem (39) with given $\{\mathbf{w}_k^{i+1}, \mathbf{v}^{i+1}, \phi_1^{i+1}, \phi_2^i\}$;
6: **Caculate** R_s^{i+1} and **set** $i = i + 1$;
7: **Until** $|R_s^i - R_s^{i-1}| < \varepsilon$ or $i > L$;
8: **Output** the optimal $\{\mathbf{w}_k^*, \mathbf{v}^*, \phi_1^*, \phi_2^*\}$.

Algorithm 3: The AO algorithm for problem (11).

3.5. Extension to Discrete Phase Shift. Due to hardware cost and power consumption limitations, practical systems adopt discrete phase shifter rather than ideal continuous phase shifter. We assume the values of discrete phase shifter are equally distributed along the unit circle $\phi_m = e^{j\varphi_m}$. In this case, the B-bit discrete phase shift set can be denoted as follows:

$$D_B = \left\{ \phi_m | \phi_m = e^{j\varphi_m}, \varphi_m \in \left\{ 0, e^{\frac{2\pi}{2^B}} \ldots e^{\frac{2\pi(2^B-1)}{2^B}} \right\} \right\}. \tag{41}$$

Then, the optimal discrete phase shifts, which are denoted as $\psi^* = e^{j\theta_{q^*}}$, can be obtained by projecting the continuous phase shifts ϕ to D_B, i.e.,

$$q^* = \arg\min_{0 \le q \le 2^B - 1} \left| \phi - e^{\frac{j2\pi q}{2^B}} \right|, \tag{42}$$

where q is an integer. It is important to note that the project operation should be conducted during each iteration of the AO algorithm instead of just at the end of the AO algorithm.

3.6. Convergence and Complexity Analysis

3.6.1. Convergence Analysis. We provide Theorem 1 to demonstrate the convergence of the proposed AO approach.

Theorem 1. *The value of the sequence* $R_s(\mathbf{w}_k^i, \mathbf{v}^i, \widehat{\phi}_1^i, \widehat{\phi}_2^i)$ *increases with iteration number i and can converge to KKT point of problem (11).*

Proof. Please see Appendix B. □

3.6.2. Complexity Analysis. Here, we examine the computational complexity cost by the suggested algorithms. The proposed AO approach is a double-layer algorithm, where the inner layer consists of subsequently optimizing $\{\mathbf{w}_k^i, \mathbf{v}^i\}$, $\widehat{\phi}_1^i$ and $\widehat{\phi}_2^i$ while the outer layer is the AO iteration. Since the complexity of optimizing $\{\mathbf{w}_k^i, \mathbf{v}^i\}$ is significant lower than that of optimizing $\widehat{\phi}_1^i$ and $\widehat{\phi}_2^i$. Therefore, the complexity of the inner layer consists of the ADMM method. During each iteration of the ADMM method, the complexity is dominant by calculating $\mathbf{a}$ which consists of calculating $(\tau\mathbf{I} + 2\mathbf{A})^{-1}$ with complexity $\mathcal{O}(N^3)$ and other multiplication operations with of $\mathcal{O}(N^2)$. However, we note that $(\tau\mathbf{I} + 2\mathbf{A})^{-1}$ only need to be calculated once and stored for other iterations, thus the complexity cost by the ADMM method is $\mathcal{O}(T_{ADMM}N^2 + N^3)$, where T_{ADMM} is the number of iterations in the ADMM method [39]. The total complexity of the proposed AO algorithm depends on the AO iteration times T_{AO} and the complexity of inner layer, which is given as $\mathcal{O}(T_{AO}(\sum_{i=1}^{2}(T_{ADMMi}M_i^2 + M_i^3)))$.

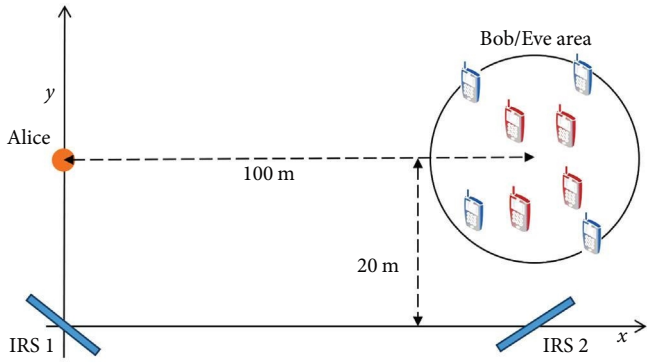

Figure 2: Simulation setup.

4. Simulation Results

This part provides extensive numerical results to examine the performance of the proposed system design. Figure 2 illustrates the top view of the simulation scenario, where the BS is located at (0, 20 m), and the IRS1 and IRS2 are located at (0, 0 m) and (100, 0 m), respectively. Additionally, the coordinates of Bobs are randomly scattered within a circle of radius 10 m and centered at (100, 20 m), and each Eve is randomly distributed within a circle of radius 10 m and centered at each Bob. The height of the BS and IRSs is set as 20 m, while the height of Bob and Eve is set as 1.5 m. The large-scale path loss is modeled as $\mathrm{PL} = \mathrm{PL}_0(d/d_0)^{-\alpha}$, where $\mathrm{PL}_0 = -30$ dB is the path loss at the reference distance $d_0 = 1$ m, d is the link distance in meters. The path loss exponent between the BS and Bobs/Eves is set as $\alpha_d = 4$, while that of IRS-related links is set as $\alpha_r = 2.2$. The Ricean factor κ for the link of BS-IRS2 and IRS1-Bobs/Eves is set to -5 dB due to obstacles in the paths, while that of the other links is set to 5 dB. Unless otherwise stated, we set $N = M_1 = M_2 = 40$, $B = 2$, $P_t^{\max} = 10$ dBm $\sigma_{b,k}^2 = \sigma_{e,k}^2 = -90$ dBm.

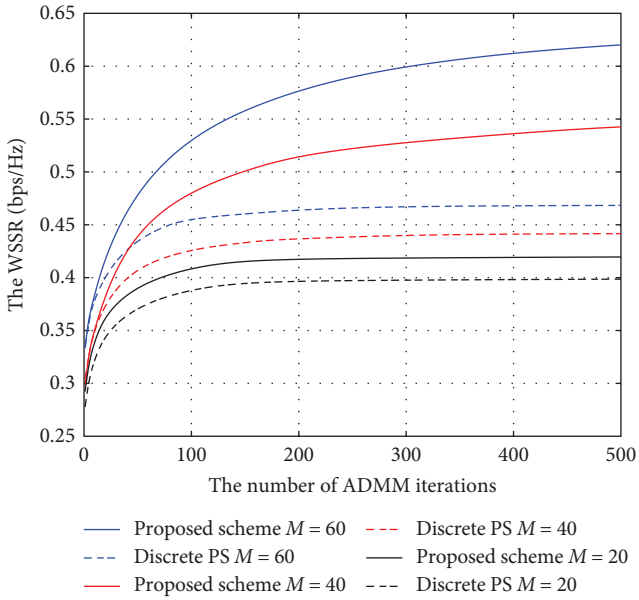

FIGURE 3: Convergence behavior of the ADMM algorithm.

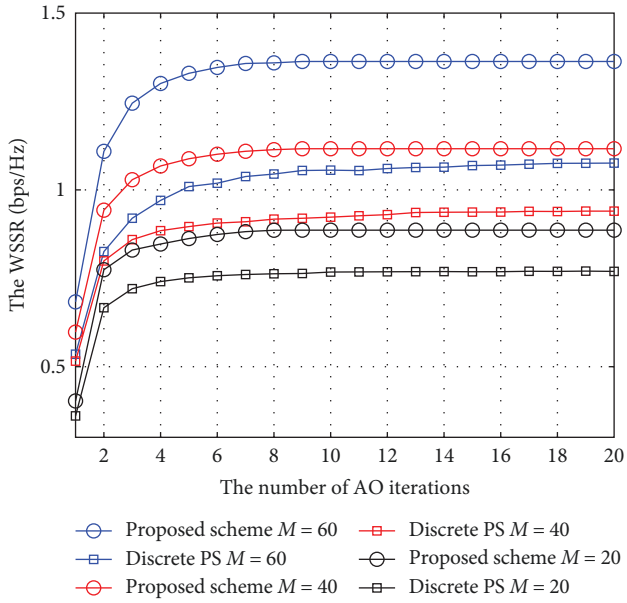

FIGURE 4: Convergence behavior of the AO algorithm.

4.1. Convergence Behavior. To begin with, we plot the convergence properties of the proposed algorithm for different amount of phase shifts $M = M_1 = M_2$ in both continuous phase shift and discrete phase shift cases. As depicted in Figure 3, it is evident that the WSSR obtained in all schemes first increases with the ADMM iteration times and then gradually converges within 500 iterations, which verifies the algorithm converges efficiently in both continuous and discrete cases. Besides, more iterations are required to converge for a larger number of IRS phase shifts, which is due to the fact that more variables need to be optimized. Next, we investigate the convergence behavior of the AO algorithm in Figure 4. Also, the WSSR first increases and then saturates with the AO iteration numbers. For all tested cases, the WSSR can achieve convergence within almost 10 iteration times, which verifies that the proposed algorithm converges fast.

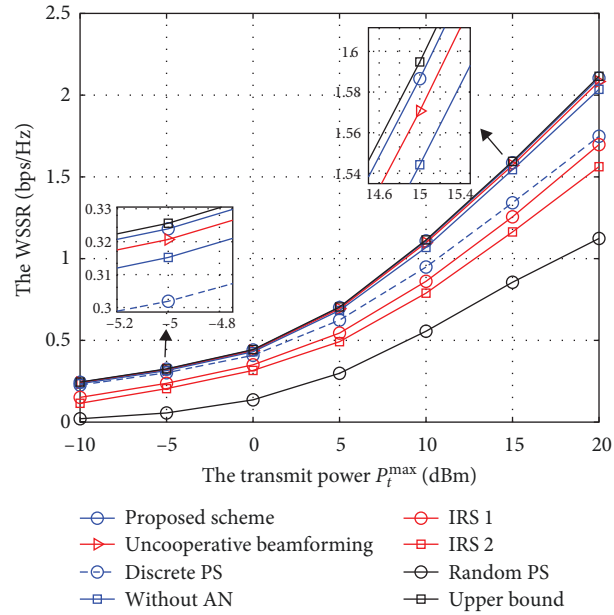

FIGURE 5: The WSSR versus the BS transmit power $P_t^{\max}$.

4.2. Performance Evaluation. In this part, we study the secure performance of the proposed cooperative double-IRS-assisted system. To facilitate a comprehensive comparison, the following approaches are employed as benchmarks: (1) uncooperative beamforming, which performs beamforming when setting $\mathbf{F} = \mathbf{0}$; (2) discrete phase shift; (3) cooperative beamforming without AN; (4) only IRS 1 is deployed near the BS; (5) only IRS 2 is deployed near the users; (6) generating the phase shift randomly; (7) adopting SDR and Gaussian randomization techniques to design the phase shift. These schemes are labeled as "Uncooperative beamforming," "Discrete PS," "Without AN," "IRS 1," "IRS 2," "Random PS," and "Upper bound," respectively.

Figure 5 illustrates the relationship between the WSSR and the maximum transmit power $P_t^{\max}$ at BS. It can be seen that the WSSR obtained in all approaches increases with the transmit power. To be specific, the proposed scheme achieves comparable performance to the upper bound scheme, while significantly reducing computational complexity, which validates its effectiveness. Besides, the performance of the proposed scheme outperforms that of "Uncooperative beamforming" scheme and single-IRS schemes ("IRS 1" and "IRS 2"), and the performance gap widens with the increase in transmit power, thus demonstrating the advantage of cooperative double-IRS framework. This observation is expected since the distributed IRS deployment with cooperative beamforming provides more spatial multiplexing gain than single-IRS. Moreover, the relatively small performance difference between the proposed scheme and the discrete phase shift scheme suggests the feasibility of the proposed algorithm. In addition, the WSSR obtained in a continuous phase scheme is significantly better than that of a random

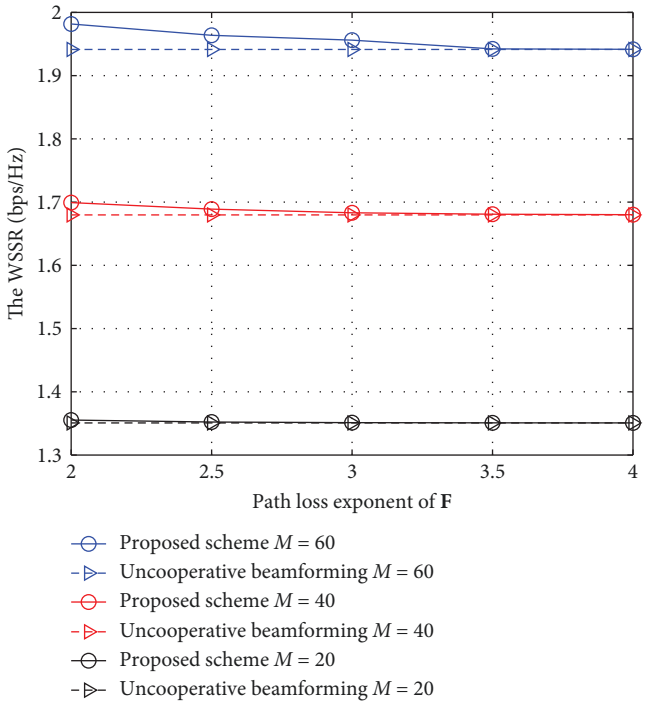

FIGURE 6: The WSSR versus the path loss exponent of channel **F**.

phase scheme, which is mainly thanks to the passive beamforming gain offered by the proposed algorithm.

To further investigate the performance of cooperative beamforming, Figure 6 shows the WSSR versus the path loss exponent of channel **F** with different number of IRS elements when $P_t^{\max} = 20$ dBm. It can be seen that the WSSR achieved by the proposed scheme decreases with the increase of path loss exponent of **F**, which is expected since more cooperative beamforming gain can be obtained when the inter-IRS channel **F** has better condition. Besides, the proposed schemes always achieve better performance than the "Uncooperative beamforming" scheme, and the advantage of cooperative beamforming increases with the number of reflective elements.

Figure 7 depicts the WSSR versus the total number of IRS elements. We can observe that the WSSR of all schemes increases with M, which is because as M increases, the IRS can provide more array gain. Moreover, the growth rate of double-IRS scheme is higher than that of single-IRS. For example, when the number of IRS elements increases from 20 to 100, the growth rate of the WSSR in the continuous phase scheme exceeds 90% (from 0.62 to 1.2 bps/Hz), while the growth rate of the WSSR in the IRS 1 and IRS 2 cases are only 80% (from 0.52 to 0.94 bps/Hz) and 50% (from 0.43 to 0.64 bps/Hz), respectively. Based on the observations, it can be suggested that as the total number of IRS elements increases, the advantages of using a cooperative double-IRS system become more significant. Besides, we observe that the WSSR without AN case is consistently lower than that of the continuous phase case, and the difference between the two increases as M grows. This finding indicates that the benefits

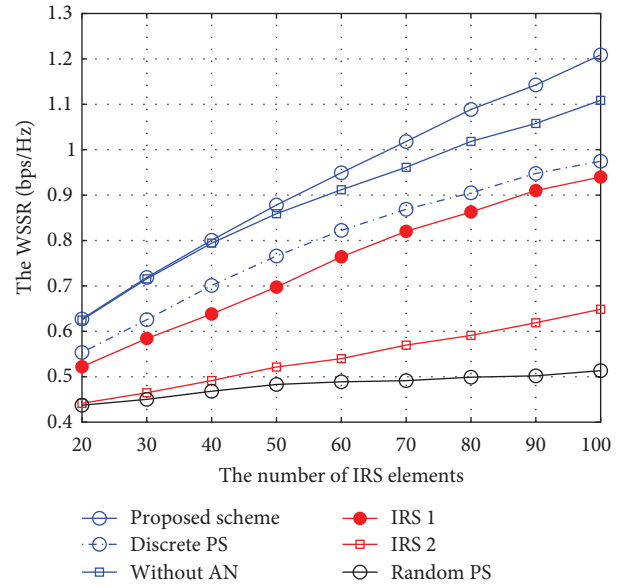

FIGURE 7: The WSSR versus the total number of IRS elements M, where $M_1 = M_2 = M/2$.

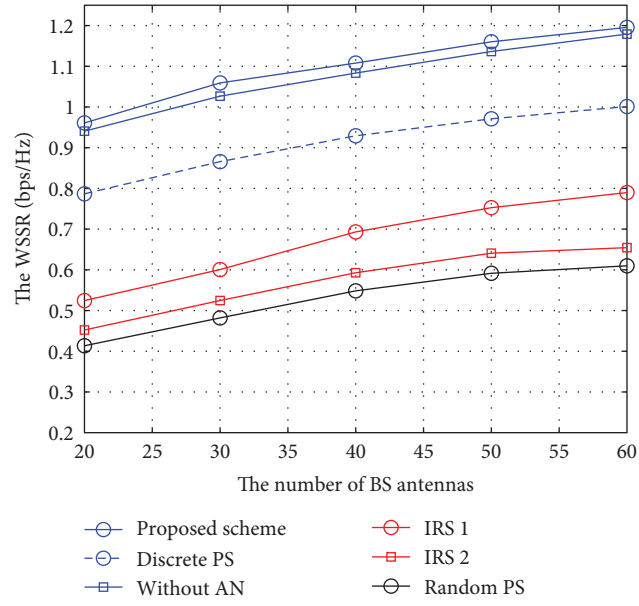

FIGURE 8: The WSSR versus the number of BS antennas N.

of AN become more prominent when the number of IRS elements is relatively large. Then, we investigate the effect of the number of BS antennas N on the WSSR in Figure 8. As expected, the WSSR for all schemes increases with N due to the availability of more spatial degrees of freedom.

Figure 9 illustrates the WSSR versus the number of Bobs/Eves K when $P_t^{\max} = 20$ dBm. As we can see that the WSSR of all schemes exhibits a downward trend as K increases. This is mainly because the interuser interference increases as the number of users grows, and the weight factor is $1/k$. Besides, we note that the performance gap between without AN

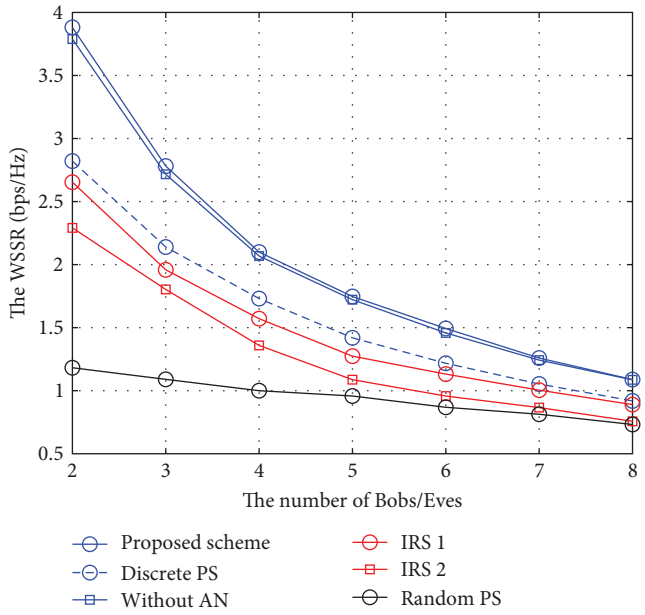

FIGURE 9: The WSSR versus the number of Bobs/Eves K.

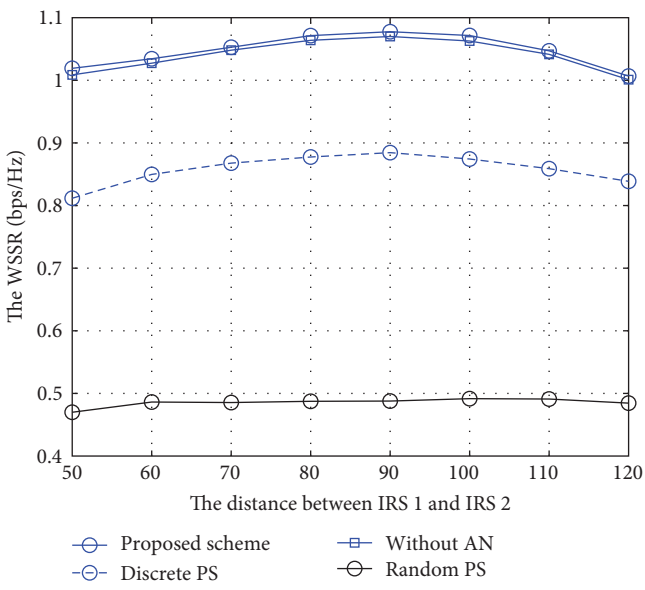

FIGURE 10: The WSSR versus the distance between IRS 1 and IRS 2.

scheme and proposed scheme becomes smaller with the increase of K. This is because the inter-user interference functions similarly to AN. As a result, the effectiveness of AN is limited in MU system, particularly when the number of users is large.

Then in Figure 10, the WSSR versus the distance between the double-IRS is depicted to show the influence of IRS deployment on the secure performance. Assuming the spacing between IRS 1 and IRS 2 is D m, then the x coordinate of IRS 1 and IRS 2 are given as $(50 - D/2)$ m and $(50 + D/2)$ m, respectively. We can observe that the WSSR first raises then reduces as D grows, and there exists an optimal value of spacing between the two IRSs, which reveals us a practical insight into deploying IRSs.

5. Conclusion

This paper investigated the cooperative beamforming of double-IRS in the MU-MISO secure system. We established the WSSR maximization problem by jointly optimizing the beamforming for transmitted signal and AN as well as the phase shifts of two cooperative IRSs. We proposed a novel SCA approach to convexify the objective function and developed an efficient AO algorithm based on the Lagrange dual method, KKT conditions, and ADMM method. At last, simulation results confirmed the significant advantages of the proposed method over benchmark schemes. For future research, we aim to investigate the user fairness and evaluate the performance of ultra-massive MIMO and THz communications in the considered system.

Appendix

A. Proof of Lemma 1

According to Nasir et al. [40], for any $u \in \mathbb{C}$, $u^t \in \mathbb{C}$, $v > 0$, and $v^t > 0$, the following inequality holds true

$$\ln\left(1+\frac{|u|^2}{v}\right) \geq \ln\left(1+\frac{|u^t|^2}{v^t}\right) - \frac{|u^t|^2}{v^t} + \frac{2\Re\{(u^t)^* u\}}{v^t} - \frac{|u^t|^2(v+|u|^2)}{v^t(v^t+|u^t|^2)}. \tag{A.1}$$

Since $R_{b,k}$ can be represented as follows:

$$R_{b,k} = \left(1 + |x_k|^2/y_k\right). \tag{A.2}$$

The inequality (9) can be proved by substituting Equation (A.1) into Equation (A.2). Next, we will prove inequality (10), which follows the similar step to [35]. We first rewrite $-R_{e,k}$ as follows:

$$-R_{e,k} = -\ln(1+z_k) + \ln\left(1+\sum_{i=1,i\neq k}^{K}\left|\widehat{\boldsymbol{\phi}}^{\mathrm{H}}\widetilde{\mathbf{g}}_k\mathbf{w}_i\right|^2 + \left|\widehat{\boldsymbol{\phi}}^{\mathrm{H}}\widehat{\mathbf{g}}_k\mathbf{v}\right|^2\right). \tag{A.3}$$

Since $-\ln(1+z_k)$ is a convex function, we can drive the lower bound by the first-order condition of the convex function.

$$-\ln(1+z_k) \geq -\ln\left(1+z_k^t\right) - \frac{1+z_k}{1+z_k^t} + 1. \tag{A.4}$$

Let $v = v^t = 1$, (A.1) can be recast as follows:

$$\ln(1+|u|^2) \geq \ln(1+|u^t|^2) - |u^t|^2 + 2\Re\{(u^t)^* u\} - \frac{|u^t|^2(1+|u|^2)}{1+|u^t|^2}. \tag{A.5}$$

Then by keeping u_i $\forall i \neq k$ fixed, we obtain the following inequality:

$$\ln(U+|u_k|^2) \geq \ln\left(U+\left|u_k^t\right|^2\right) - \left|u_k^t\right|^2, \tag{A.6}$$

$$+2\Re\left\{\left(u_k^t\right)^* u_k\right\} - \frac{\left|u_k^t\right|^2(U+|u_k|^2)}{U+\left|u_k^t\right|^2}, \tag{A.7}$$

where $U=1+\sum_{i=1,i\neq k}^{K}|u_i|^2$. Using Equation (A.6) with $k=1,\ldots,K$, the following inequality can be derived:

$$\begin{aligned}\ln\left(1+\sum_{i=1}^{K}|u_i|^2\right) &\geq \ln\left(1+\sum_{i=1}^{K}|u_i^t|^2\right) - \sum_{i=1}^{K}|u_i^t|^2 \\ &+\sum_{i=1}^{K}2\Re\{(u_i^t)^* u_i\} - \frac{\sum_{i=1}^{K}|u_i^t|^2\left(1+\sum_{i=1}^{K}|u_i|^2\right)}{\left(1+\sum_{i=1}^{K}|u_i^t|^2\right)}.\end{aligned} \tag{A.8}$$

According to Equation (A.8), we have the following:

$$\begin{aligned}\ln\Bigg(1+\sum_{i=1,i\neq k}^{K}\left|\widehat{\boldsymbol{\phi}}^{\mathrm{H}}\widetilde{\mathbf{g}}_k\mathbf{w}_i\right|^2+\left|\widehat{\boldsymbol{\phi}}^{\mathrm{H}}\widehat{\mathbf{g}}_k\mathbf{v}\right|^2\Bigg) &\geq \ln\left(1+c_k^t\right) \\ -c_k^t+2\sum_{i=1,i\neq k}^{K}\Re\left\{(\mathbf{w}_i)^{\mathrm{H}}\widetilde{\mathbf{g}}_k^{\mathrm{H}}\widehat{\boldsymbol{\phi}}\left(\widehat{\boldsymbol{\phi}}^t\right)^{\mathrm{H}}\widetilde{\mathbf{g}}_k\mathbf{w}^t\right\} \\ +2\Re\left\{(\mathbf{v})^{\mathrm{H}}\widehat{\mathbf{g}}_k^{\mathrm{H}}\widehat{\boldsymbol{\phi}}\left(\widehat{\boldsymbol{\phi}}^t\right)^{\mathrm{H}}\widehat{\mathbf{g}}_k\mathbf{v}^t\right\} \\ -\frac{c_k^t}{1+c_k^t}\left(1+\sum_{i=1,i\neq k}^{K}\left|\widehat{\boldsymbol{\phi}}^{\mathrm{H}}\widetilde{\mathbf{g}}_k\mathbf{w}_i\right|^2+\left|\widehat{\boldsymbol{\phi}}^{\mathrm{H}}\widehat{\mathbf{g}}_k\mathbf{v}\right|^2\right).\end{aligned} \tag{A.9}$$

Finally, the inequality (10) is proved by substituting Equations (A.4) and (A.9) back into Equation (A.3).

B. Proof of Theorem 1

To begin with, we will demonstrate that the objective function $R_s^i(\mathbf{w}_k,\mathbf{v},\widehat{\boldsymbol{\phi}}_1,\widehat{\boldsymbol{\phi}}_2)$ guaranteed convergence. Considering the ith iteration of Algorithm 3, an upper bound of R_s, i.e., $R_s^{ub1}(\mathbf{w}_k,\mathbf{v},\widehat{\boldsymbol{\phi}}_1^i,\widehat{\boldsymbol{\phi}}_2^i)$ around the given point $\{\mathbf{w}_k^i,\mathbf{v}^i,\widehat{\boldsymbol{\phi}}_1^i,\widehat{\boldsymbol{\phi}}_2^i\}$ is obtained in updating $\{\mathbf{w}_k^{i+1},\mathbf{v}^{i+1}\}$. Similarly, with updating $\widehat{\boldsymbol{\phi}}_1^{i+1}$ and $\widehat{\boldsymbol{\phi}}_2^{i+1}$, two upper bound of R_s^i can be obtained around the given point $\{\mathbf{w}_k^{i+1},\mathbf{v}^{i+1},\widehat{\boldsymbol{\phi}}_1^i,\widehat{\boldsymbol{\phi}}_2^i\}$ and $\{\mathbf{w}_k^{i+1},\mathbf{v}^{i+1},\widehat{\boldsymbol{\phi}}_1^{i+1},\widehat{\boldsymbol{\phi}}_2^i\}$, which can be denoted as $R_s^{ub2}(\mathbf{w}_k^{i+1},\mathbf{v}^{i+1},\widehat{\boldsymbol{\phi}}_1,\widehat{\boldsymbol{\phi}}_2^i)$ and $R_s^{ub3}(\mathbf{w}_k^{i+1},\mathbf{v}^{i+1},\widehat{\boldsymbol{\phi}}_1^{i+1},\widehat{\boldsymbol{\phi}}_2)$. Thus, we have the following inequality:

$$\begin{aligned}R_s\left(\mathbf{w}_k^i,\mathbf{v}^i,\widehat{\boldsymbol{\phi}}_1^i,\widehat{\boldsymbol{\phi}}_2^i\right) &\leq \max_{\mathbf{w}_k,\mathbf{v}} R_s^{ub1}\left(\mathbf{w}_k,\mathbf{v},\widehat{\boldsymbol{\phi}}_1^i,\widehat{\boldsymbol{\phi}}_2^i\right) \\ &\underset{(a)}{\leq} \max_{\widehat{\boldsymbol{\phi}}_1} R_s^{ub2}\left(\mathbf{w}_k^{i+1},\mathbf{v}^{i+1},\widehat{\boldsymbol{\phi}}_1,\widehat{\boldsymbol{\phi}}_2^i\right) \\ &\underset{(b)}{\leq} \max_{\widehat{\boldsymbol{\phi}}_2} R_s^{ub3}\left(\mathbf{w}_k^{i+1},\mathbf{v}^{i+1},\widehat{\boldsymbol{\phi}}_1^{i+1},\widehat{\boldsymbol{\phi}}_2\right) \\ &\underset{(c)}{\leq} R_s\left(\mathbf{w}_k^{i+1},\mathbf{v}^{i+1},\widehat{\boldsymbol{\phi}}_1^{i+1},\widehat{\boldsymbol{\phi}}_2^{i+1}\right),\end{aligned} \tag{B.1}$$

where (a, b, c) holds due to the fact that $\{\mathbf{w}_k^{i+1},\mathbf{v}^{i+1}\}$, $\widehat{\boldsymbol{\phi}}_1^{i+1}$, and $\widehat{\boldsymbol{\phi}}_2^{i+1}$ are the optimal solution of the problems (12), (22), and (39), respectively. Meanwhile, note that the feasible set is bounded by the constraints (8b) and (8c). Therefore, according to the Cauchy theorem, the sequence $\{\mathbf{w}_k^i,\mathbf{v}^i,\widehat{\boldsymbol{\phi}}_1^i,\widehat{\boldsymbol{\phi}}_2^i\}$ can always converge to a local optimum as $i\to\infty$.

Next, we will demonstrate the optimal point obtained by Algorithm 3 is a KKT point. We first write the Lagrangian function of Equation (12) as follows:

$$\begin{aligned}\mathscr{L}_1\left(\mathbf{w}_k,\mathbf{v},\widehat{\boldsymbol{\phi}}_1^i,\widehat{\boldsymbol{\phi}}_2^i,\lambda\right) &= R_s^{ub1}\left(\mathbf{w}_k,\mathbf{v},\widehat{\boldsymbol{\phi}}_1^i,\widehat{\boldsymbol{\phi}}_2^i\right) \\ &+\widehat{\lambda}\left(\sum_{k=1}^{K}\|\mathbf{w}_k\|^2+\|\mathbf{v}\|^2-P_t^{\max}\right),\end{aligned} \tag{B.2}$$

where $\widehat{\lambda}\geq 0$ is the dual variable of Equation (12b). When $i\to\infty$, the involving KKT conditions can be written as follows:

$$\nabla_{\mathbf{w}_k}R_s^{ub1}\left(\mathbf{w}_k^*,\mathbf{v}^*,\widehat{\boldsymbol{\phi}}_1^i,\widehat{\boldsymbol{\phi}}_2^i\right)+2\widehat{\lambda}^*\mathbf{w}_k^*=0,\forall k, \tag{B.3}$$

$$\nabla_{\mathbf{v}}R_s^{ub1}\left(\mathbf{w}_k^*,\mathbf{v}^*,\widehat{\boldsymbol{\phi}}_1^i,\widehat{\boldsymbol{\phi}}_2^i\right)+2\widehat{\lambda}^*\mathbf{v}^*=0, \tag{B.4}$$

$$\widehat{\lambda}^*\left(\sum_{k=1}^{K}\|\mathbf{w}_k\|^2+\|\mathbf{v}\|^2-P_t^{\max}\right)=0. \tag{B.5}$$

Meanwhile, the Lagrange function of Equation (23) can be written as follows:

$$\begin{aligned}\mathscr{L}_2\left(\mathbf{w}_k^i,\mathbf{v}^i,\widehat{\boldsymbol{\phi}}_1,\widehat{\boldsymbol{\phi}}_2^i,\varsigma\right) &= R_s^{ub2}\left(\mathbf{w}_k^i,\mathbf{v}^i,\widehat{\boldsymbol{\phi}}_1,\widehat{\boldsymbol{\phi}}_2^i\right) \\ &+\sum_{m=1}^{M_1}\varsigma_m\left(\left[\widehat{\boldsymbol{\phi}}_1\right]_m^{\dagger}\left[\widehat{\boldsymbol{\phi}}_1\right]_m-1\right),\end{aligned} \tag{B.6}$$

where $\varsigma=[\varsigma_1\geq 0,\ldots,\varsigma_{M_1}\geq 0]$ is the dual variable of $\widehat{\boldsymbol{\phi}}_1$. The corresponding KKT conditions are given as follows:

$$\nabla_{\left[\widehat{\boldsymbol{\phi}}_1\right]_m}R_s^{ub2}\left(\mathbf{w}_k^i,\mathbf{v}^i,\widehat{\boldsymbol{\phi}}_1^*,\widehat{\boldsymbol{\phi}}_2^i\right)+\varsigma_m^*\left[\widehat{\boldsymbol{\phi}}_1\right]_m^{\dagger}=0,\forall m, \tag{B.7}$$

$$\varsigma_m^*\left(\left[\widehat{\boldsymbol{\phi}}_1^*\right]_m^{\dagger}\left[\widehat{\boldsymbol{\phi}}_1^*\right]_m-1\right)=0,\forall m. \tag{B.8}$$

The KKT condition for $\widehat{\boldsymbol{\phi}}_2$ can be derived similarly. The above KKT conditions hold since $\{\mathbf{w}_k^*,\mathbf{v}^*\}$, $\widehat{\boldsymbol{\phi}}_1^*$ and $\widehat{\boldsymbol{\phi}}_2^*$ are the optimal solutions of Equations (12), (23), and (39), respectively. Therefore, $\{\mathbf{w}_k^*,\mathbf{v}^*,\widehat{\boldsymbol{\phi}}_1^*,\widehat{\boldsymbol{\phi}}_2^*\}$ is KKT point of problem (11).

Data Availability

Data will be available upon reasonable request.

Conflicts of Interest

The authors declare that they have no conflicts of interest.

Acknowledgments

This research was funded in part by the National Key Research and Development Program of China (no.2022YFB2902205), in part by the National Natural Science Foundation of China under grant (nos. U22A2001 and 61901490), in part by the Training Program for Young Scholar of Henan Province for Colleges and Universities under grant 2020GGJS172, in part by the Program for Science & Technology Innovation Talents in Universities of Henan Province under grant 22HASTIT020, in part by the Scientific and Technological Key Project of Henan Province under grant 232102210151. The work of Zheng Chu was supported in part by the Open Fund of the Shaanxi Key Laboratory of Information Communication Network and Security under grant ICNS201801. The work of Li Zhen was supported in part by the Innovation Capability Support Program of Shaanxi under grant 2023KJXX-062, in part by the Key Research and Development Program of Shaanxi under grant 2024GX-YBXM-064, and in part by the Scientific Research Program of Shaanxi Provincial Education Department under grant 23JS057.

References

[1] C.-X. Wang, X. You, X. Gao et al., "On the road to 6G: visions, requirements, key technologies, and testbeds," *IEEE Communications Surveys & Tutorials*, vol. 25, no. 2, pp. 905–974, 2023.

[2] R. W. Heath, N. Gonzalez-Prelcic, S. Rangan, W. Roh, and A. M. Sayeed, "An overview of signal processing techniques for millimeter wave MIMO systems," *IEEE Journal of Selected Topics in Signal Processing*, vol. 10, no. 3, pp. 436–453, 2016.

[3] Q. Wu and R. Zhang, "Towards smart and reconfigurable environment: intelligent reflecting surface aided wireless network," *IEEE Communications Magazine*, vol. 58, no. 1, pp. 106–112, 2020.

[4] Q. Wu, S. Zhang, B. Zheng, C. You, and R. Zhang, "Intelligent reflecting surface-aided wireless communications: a tutorial," *IEEE Transactions on Communications*, vol. 69, no. 5, pp. 3313–3351, 2021.

[5] E. Basar, M. Di Renzo, J. De Rosny, M. Debbah, M.-S. Alouini, and R. Zhang, "Wireless communications through reconfigurable intelligent surfaces," *IEEE Access*, vol. 7, pp. 116753–116773, 2019.

[6] C. Huang, A. Zappone, G. C. Alexandropoulos, M. Debbah, and C. Yuen, "Reconfigurable intelligent surfaces for energy efficiency in wireless communication," *IEEE Transactions on Wireless Communications*, vol. 18, no. 8, pp. 4157–4170, 2019.

[7] Z. Chu, W. Hao, P. Xiao, and J. Shi, "Intelligent reflecting surface aided multi-antenna secure transmission," *IEEE Wireless Communications Letters*, vol. 9, no. 1, pp. 108–112, 2020.

[8] M. Hua and Q. Wu, "Throughput maximization for IRS-aided MIMO FD-WPCN with non-linear EH model," *IEEE Journal of Selected Topics in Signal Processing*, vol. 16, no. 5, pp. 918–932, 2022.

[9] W. Hao, F. Zhou, M. Zeng, O. A. Dobre, and N. Al-Dhahir, "Ultra wideband THz IRS communications: applications, challenges, key techniques, and research opportunities," *IEEE Network*, vol. 36, no. 6, pp. 214–220, 2022.

[10] M. Hua, Q. Wu, W. Chen, O. A. Dobre, and A. L. Swindlehurst, "Secure intelligent reflecting surface aided integrated sensing and communication," *IEEE Transactions on Wireless Communications*, vol. 23, no. 1, pp. 575–591, 2024.

[11] M. Hua, Q. Wu, C. He, S. Ma, and W. Chen, "Joint active and passive beamforming design for IRS-aided radar-communication," *IEEE Transactions on Wireless Communications*, vol. 22, no. 4, pp. 2278–2294, 2023.

[12] X. You, C.-X. Wang, J. Huang et al., "Towards 6G wireless communication networks: vision, enabling technologies, and new paradigm shifts," *Science China Information Sciences*, vol. 64, Article ID 110301, 2021.

[13] C. Huang, G. Chen, and K.-K. Wong, "Multi-agent reinforcement learning-based buffer-aided relay selection in IRS-assisted secure cooperative networks," *IEEE Transactions on Information Forensics and Security*, vol. 16, pp. 4101–4112, 2021.

[14] Z. Chu, W. Hao, P. Xiao et al., "Secrecy rate optimization for intelligent reflecting surface assisted MIMO system," *IEEE Transactions on Information Forensics and Security*, vol. 16, pp. 1655–1669, 2021.

[15] F. Zhao, W. Hao, H. Guo, G. Sun, Y. Wang, and H. Zhang, "Secure energy efficiency for mmwave-NOMA cognitive satellite terrestrial network," *IEEE Communications Letters*, vol. 27, no. 1, pp. 283–287, 2023.

[16] M. Hua, Y. Wang, Q. Wu, H. Dai, Y. Huang, and L. Yang, "Energy-efficient cooperative secure transmission in multi-UAV-enabled wireless networks," *IEEE Transactions on Vehicular Technology*, vol. 68, no. 8, pp. 7761–7775, 2019.

[17] S. Fang, G. Chen, and Y. Li, "Joint optimization for secure intelligent reflecting surface assisted UAV networks," *IEEE Wireless Communications Letters*, vol. 10, no. 2, pp. 276–280, 2021.

[18] J. Yuan, G. Chen, M. Wen, R. Tafazolli, and E. Panayirci, "Secure transmission for THz-empowered RIS-assisted non-terrestrial networks," *IEEE Transactions on Vehicular Technology*, vol. 72, no. 5, pp. 5989–6000, 2023.

[19] W. Hao, J. Li, G. Sun, M. Zeng, and O. A. Dobre, "Securing reconfigurable intelligent surface-aided cell-free networks," *IEEE Transactions on Information Forensics and Security*, vol. 17, pp. 3720–3733, 2022.

[20] Z. Chu, P. Xiao, D. Mi, W. Hao, Y. Xiao, and L.-L. Yang, "Multi-IRS assisted multi-cluster wireless powered IoT networks," *IEEE Transactions on Wireless Communications*, vol. 22, no. 7, pp. 4712–4728, 2023.

[21] W. Mei, B. Zheng, C. You, and R. Zhang, "Intelligent reflecting surface-aided wireless networks: From single-reflection to multireflection design and optimization," *Proceedings of the IEEE*, vol. 110, no. 9, pp. 1380–1400, 2022.

[22] Y. Han, S. Zhang, L. Duan, and R. Zhang, "Cooperative double-IRS aided communication: beamforming design and power scaling," *IEEE Wireless Communications Letters*, vol. 9, no. 8, pp. 1206–1210, 2020.

[23] Y. Han, S. Zhang, L. Duan, and R. Zhang, "Double-IRS aided MIMO communication under LoS channels: capacity maximization and scaling," *IEEE Transactions on Communications*, vol. 70, no. 4, pp. 2820–2837, 2022.

[24] X. Chen, H. Xu, G. Zhang, A. Zhou, L. Zhao, and Z. Wang, "Cooperative beamforming design for double-IRS-assisted

MISO communication system," *Physical Communication*, vol. 55, Article ID 101826, 2022.
[25] B. Zheng, C. You, and R. Zhang, "Double-IRS assisted multi-user MIMO: cooperative passive beamforming design," *IEEE Transactions on Wireless Communications*, vol. 20, no. 7, pp. 4513–4526, 2021.
[26] H. Niu, Z. Chu, F. Zhou, C. Pan, D. W. K. Ng, and H. X. Nguyen, "Double intelligent reflecting surface-assisted multi-user MIMO mmwave systems with hybrid precoding," *IEEE Transactions on Vehicular Technology*, vol. 71, no. 2, pp. 1575–1587, 2022.
[27] Z. Zhang and Z. Zhao, "Weighted sum-rate maximization for multi-hop RIS-aided multi-user communications: a minorization-maximization approach," in *2021 IEEE 22nd International Workshop on Signal Processing Advances in Wireless Communications (SPAWC)*, pp. 106–110, IEEE, Lucca, Italy, 2021.
[28] C. Lu, Y. Fang, and L. Qiu, "Energy-efficient beamforming design for cooperative double-IRS aided multi-user MIMO," in *GLOBECOM 2022-2022 IEEE Global Communications Conference*, pp. 4619–4624, IEEE, Rio de Janeiro, Brazil, 2022.
[29] L. Dong, H.-M. Wang, J. Bai, and H. Xiao, "Double intelligent reflecting surface for secure transmission with inter-surface signal reflection," *IEEE Transactions on Vehicular Technology*, vol. 70, no. 3, pp. 2912–2916, 2021.
[30] Y. Wen, G. Chen, S. Fang, Z. Chu, P. Xiao, and R. Tafazolli, "STAR-RIS-assisted-full-duplex jamming design for secure wireless communications system," 2023.
[31] G. Chen, Y. Gong, P. Xiao, and J. A. Chambers, "Physical layer network security in the full-duplex relay system," *IEEE Transactions on Information Forensics and Security*, vol. 10, no. 3, pp. 574–583, 2015.
[32] M. Cui, G. Zhang, and R. Zhang, "Secure wireless communication via intelligent reflecting surface," *IEEE Wireless Communications Letters*, vol. 8, no. 5, pp. 1410–1414, 2019.
[33] B. Zheng, C. You, and R. Zhang, "Efficient channel estimation for double-IRS aided multi-user MIMO system," *IEEE Transactions on Communications*, vol. 69, no. 6, pp. 3818–3832, 2021.
[34] W. Du, Z. Chu, G. Chen et al., "Weighted sum-rate and energy efficiency maximization for joint ITS and IRS assisted multiuser MIMO networks," *IEEE Transactions on Communications*, vol. 70, no. 11, pp. 7351–7364, 2022.
[35] H. Niu, Z. Lin, Z. Chu et al., "Joint beamforming design for secure RIS-assisted IoT networks," *IEEE Internet of Things Journal*, vol. 10, no. 2, pp. 1628–1641, 2023.
[36] M. Grant and S. P. Boyd, "CVX: Matlab software for disciplined convex programming," 2014, [Online]. Available: http://cvxr.com/cvx.
[37] Q. Wu and R. Zhang, "Intelligent reflecting surface enhanced wireless network: joint active and passive beamforming design," in *2018 IEEE Global Communications Conference (GLOBECOM)*, pp. 1–6, IEEE, Abu Dhabi, United Arab Emirates, 2018.
[38] H. Niu, Z. Chu, F. Zhou, Z. Zhu, M. Zhang, and K.-K. Wong, "Weighted sum secrecy rate maximization using intelligent reflecting surface," *IEEE Transactions on Communications*, vol. 69, no. 9, pp. 6170–6184, 2021.
[39] Q. Li, C. Li, and J. Lin, "Constant modulus secure beamforming for multicast massive MIMO wiretap channels," *IEEE Transactions on Information Forensics and Security*, vol. 15, pp. 264–275, 2020.
[40] A. A. Nasir, H. D. Tuan, T. Q. Duong, and H. V. Poor, "Secrecy rate beamforming for multicell networks with information and energy harvesting," *IEEE Transactions on Signal Processing*, vol. 65, no. 3, pp. 677–689, 2017.